

CBGBENCH: FILL IN THE BLANK OF PROTEIN-MOLECULE COMPLEX BINDING GRAPH

Haitao Lin^{1,3,†}, Guojiang Zhao^{2,†}, Odin Zhang³, Yufei Huang¹,
Lirong Wu¹, Zicheng Liu¹, Siyuan Li¹, Cheng Tan¹, Zhifeng Gao², Stan Z. Li^{1,*}

¹ AI Lab, Research Center for Industries of the Future, Westlake University;

² DP Technology; ³ Zhejiang University; [†] Equal Contribution; ^{*} Corresponding Author.
linhaitao@westlake.edu.cn

ABSTRACT

Structure-based drug design (SBDD) aims to generate potential drugs that can bind to a target protein and is greatly expedited by the aid of AI techniques in generative models. However, a lack of systematic understanding persists due to the diverse settings, complex implementation, difficult reproducibility, and task singularity. Firstly, the absence of standardization can lead to unfair comparisons and inconclusive insights. To address this dilemma, we propose CBGBench, a comprehensive benchmark for SBDD, that unifies the task as a generative graph completion, analogous to fill-in-the-blank of the 3D complex binding graph. By categorizing existing methods based on their attributes, CBGBench facilitates a modular and extensible framework that implements various cutting-edge methods. Secondly, a single de novo molecule generation task can hardly reflect their capabilities. To broaden the scope, we adapt these models to a range of tasks essential in drug design, considered sub-tasks within the graph fill-in-the-blank tasks. These tasks include the generative designation of de novo molecules, linkers, fragments, scaffolds, and sidechains, all conditioned on the structures of protein pockets. Our evaluations are conducted with fairness, encompassing comprehensive perspectives on interaction, chemical properties, geometry authenticity, and substructure validity. We further provide deep insights with analysis from empirical studies. Our results indicate that there is potential for further improvements on many tasks, with optimization in network architectures, and effective incorporation of chemical prior knowledge. Finally, to lower the barrier to entry and facilitate further developments in the field, we also provide a single codebase (<https://github.com/EDAPINENUT/CBGBench>) that unifies the discussed state-of-the-art models, data pre-processing, training, sampling, and evaluation.

1 INTRODUCTION

The rapid and remarkable progress in Graph Neural Networks (GNNs) and generative models have advanced the bio-molecule design in these years (Jumper et al., 2021; Watson et al., 2023; Krishna et al., 2023). In structure-based drug design, AI-aided methods aim to learn the chemical space of the molecules that can bind to certain proteins as targets, which decreases the general chemical space of molecule compounds ($\sim 10^{60}$) to a more compact search space and enables the model to explore the potential binding drugs. Recent success in generative models such as diffusion models (Ho et al., 2020; Lipman et al., 2022; Song et al., 2020) further enhanced these methods to fully exploit the targeted chemical space, and AI-aided SBDD has been propelled into another prominence.

Despite the significance of the SBDD and the development of various approaches, there remains a lack of a comprehensive benchmark for this field covering various practical application scenarios. *On the one hand*, although different methods are proposed for the task, the experimental setup is not unified, and the evaluation protocol also differs. For example, GRAPHBP (Liu et al., 2022) use a different training and test split of Crossdocked2020 (Francoeur et al., 2020) from concurrent works like POCKET2MOL (Peng et al., 2022) and 3DSBDD (Luo et al., 2022); And DIFFBP (Lin et al., 2022) and GRAPHBP employ Gnina (McNutt et al., 2021) instead of AutoDock Vina (Trott & Olson, 2009) as the evaluator for obtaining docking score as binding affinity. Besides, the complex

implementation of models makes the modules coupled, so it is hard to figure out which proposed module contributes to the improvements in performance. For example, though TARGETDIFF (Guan et al., 2023b) and DIFFBP are both diffusion-based methods, the first one uses EGNN (Satorras et al., 2022) to predict the ground-truth position of each atom in the molecule while the later one uses GVP (Jing et al., 2020) to remove the added noise in a score-based way. To have a systematic understanding of the designation for diffusion models in molecule generation, the network architectures should be fixed to keep the expressivity equal. *On the other hand*, the task of *de novo* generation of molecules is a branch of SBDD. There are also other important tasks, such as the design of molecular side chains in lead optimization, or linker design to combine functional fragments into a single, connected molecule (Igashov et al., 2022; Guan et al., 2023a). It is highly meaningful to explore whether these methods can be successfully transferred to applications in drug optimization.

In this way, here we propose **CBGBench** as a benchmark for SBDD, with the latest state-of-the-art methods included and integrated into a single codebase (See Appendix. C for details). Firstly, we unify the generation of the binding molecule as a graph completion task, *i.e.* fill-in-the-blank of the 3D Complex Binding Graph. In this way, the systematic categorization of existing methods is based on three dichotomies: (i) voxelized *v.s.* continuous position generation, (ii) one-shot *v.s.* autoregressive generation, and (iii) domain-knowledge-based *v.s.* full-data-driven generation. As a result, the methods can be easily modularized and extensible in a unified framework. Secondly, CBGBench introduces a unified protocol with a comprehensive evaluation. In **chemical property**, the classical ones including QED, SA, LogP and LPSK are considered; For **interaction**, besides Vina energy, we extend the evaluation to interaction types between protein and molecules; For **geometry**, we considered static ones including bond length and bond angles, and clashes resulted from protein-molecule cross-clash between atoms in the generated molecules; In **substructure** analysis, we consider single atoms, rings, and functional groups as pharmacophores. Moreover, thanks to our reformulation of the problem and extensible modular implementation, we can easily extend these methods to the other four tasks in lead optimization, including the designation of (i) linkers, (ii) fragments, (iii) side chains and (iv) scaffolds. Comprehensive evaluation is also conducted for these tasks, to explore the potential application value of the existing methods in lead optimization.

As a result, several brief conclusions can be reached as the following:

- CNN-based methods by modeling voxelized density maps as molecule representations remain highly competitive in target-aware molecule generation, and the diffusion-based ones achieve the state-of-the-art.
- For autoregressive methods, it is essential to enable the model to successfully capture the patterns of chemical bonds.
- Prior knowledge has been incorporated into the model in recent works, but the improvements remain limited. Effective design of integrating physical and chemical domain knowledge remains a challenge, leaving substantial room for future research.
- Most evaluated methods can be well generalized to lead optimization. Empirical studies show that scaffold hopping is the most challenging task among them, while linker design is relatively the easiest. However, there is still a large space for improvements in these tasks.
- The conclusions drawn from the experimental results and with the evaluation protocol of CBGBench, are mainly consistent with those obtained on real-world targets, demonstrating generalizability and effectiveness of our benchmark.

2 BACKGROUND

2.1 PROBLEM STATEMENT

For a binding system composed of a protein-molecule pair as $(\mathcal{P}, \mathcal{M})$, in which \mathcal{P} contains N_{rec} atoms of proteins and \mathcal{M} contains N_{lig} atoms of molecules, we represent the index set of the protein’s atom as \mathcal{I}_{rec} and the molecule’s atoms as \mathcal{I}_{lig} , with $|\mathcal{I}_{\text{rec}}| = N_{\text{rec}}$ and $|\mathcal{I}_{\text{lig}}| = N_{\text{lig}}$. The binding graph can be regarded as a heterogeneous graph. One subgraph is protein structures, as $\mathcal{P} = (\mathbf{V}_{\text{rec}}, \mathbf{E}_{\text{rec}})$, where $\mathbf{V}_{\text{rec}} = \{(a_i, \mathbf{x}_i, s_i)\}_{i \in \mathcal{I}_{\text{rec}}}$ is the node set, and $\mathbf{E}_{\text{rec}} = \{(i, j, e_{i,j})\}_{i,j \in \mathcal{I}_{\text{rec}}}$ is the edge set. Here, a_i is the atom types with $a_i = 1, \dots, M$, $\mathbf{x}_i \in \mathbb{R}^3$ is the corresponding 3D position, and $s_i = 1, \dots, 20$ is the amino acid types that i -th atom belongs to; elements in edge set means there exists

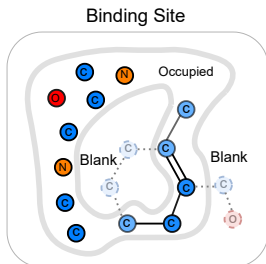


Figure 1: Filling the blank in the complex binding site.

A comparable analogy can be made that if we also divide the atoms in a molecule into known and to-be-generated parts, we can extend the aforementioned ‘filling-in-the-blank’ task as shown in Figure. 1. In specific, for the missing blanks, we write the node set for generation as $\mathcal{G} = (\mathbf{V}_{\text{gen}}, \mathbf{E}_{\text{gen}})$, and the known atoms in the molecule as elements in the context set $\mathcal{C} = (\mathbf{V}_{\text{ctx}}, \mathbf{E}_{\text{ctx}})$, in which $\mathcal{I}_{\text{ctx}} = \mathcal{I}_{\text{lig}} \setminus \mathcal{I}_{\text{gen}}$. Therefore, *the generative model for filling the blanks of the missing parts of molecules aims to learn the probability of $p(\mathcal{G}|\mathcal{C}, \mathcal{P})$* . The newly-defined task of fill-in-the-partial-graph is of great significance in SBDD, especially in lead optimization, and we establish other four sub-tasks of it besides *de novo* design, with accessible datasets in Sec. 3.

2.2 RELATED WORK AND TAXONOMY

The SBDD methods are initially combined with deep neural networks on voxel grids, such as LIGAN (Masuda et al., 2020) generating atom voxelized density maps using VAE (Kingma & Welling, 2022) and incorporating Convolutional Neural Networks (CNNs) as the architecture, and 3DSBDD (Luo et al., 2022) predicts whether the position on grids is occupied with which type of atoms in auto-regressive ways with Graph Neural Networks (GNNs). Then, the development of Equivariant Graph Neural Networks (EGNNs) boosts the SBDD methods to directly generate the continuous 3D positions, such as POCKET2MOL (Peng et al., 2022) generating the molecules’ atom types, positions, and the connected bonds and GRAPHBP (Liu et al., 2022) employing normalizing flows to generate these attributes, both in an auto-regressive way. The diffusion denoising probabilistic models (DDPM) (Ho et al., 2020) further propel the AI-aided SBDD methods, such as TARGETDIFF (Guan et al., 2023b), DIFFBP (Lin et al., 2022) and DIFFSBDD (Schneuing et al., 2022), inspired by EDM (Hoogeboom et al., 2022), generating full atoms’ positions and element types, with different diffusion models. In recent years, domain knowledge has been used to constrain or guide the generation of binding drugs. For example, FLAG (Zhang et al., 2023b) and D3FG (Lin et al., 2023) use prior knowledge of fragment motifs to model the coarse structures, which generate fragments in molecules in one-shot and auto-regressive ways, respectively; And DECOMPDIFF (Guan et al., 2023c) harnesses virtual points searching for arm- and scaffold-clustering as prior knowledge, and using multivariate Gaussian process to model atom positions in different clusters, with validity guidance for sampling. More recently, thanks to technological breakthroughs brought by generative AI, more related approaches have been proposed, which not only build upon previous modeling concepts but also incorporate new generative model techniques. MOLCRAFT (Qu et al., 2024), as the SBDD version of GEOBFN (Song et al., 2024), employs Bayesian Flow Network (Graves et al., 2024) as the variant of diffusion models, to address the continuous-discrete gap in modeling the elements’ type and atoms’ positions by applying continuous noise and smooth transformation; VOXBIND (Pinheiro et al., 2024a), following their pioneering exploration of VOXMOL (Pinheiro et al., 2024b), continues modeling the 3D voxelization of molecules in a diffusion denoising way, with walk-jump sampling method used to generate molecules. In this way, we can categorize these methods with the three standards:

- Whether the positions of atoms are generated in continuous 3D space or voxelized grids.
- Whether the generation process is auto-regressive or one-shot.
- Whether the domain knowledge is introduced to integrate extra prior into the model.

To better articulate, we classify them according to Table. 1, and Figure. 2 gives a simple demonstration of the criteria for taxonomy. A detailed review of these methods is given in Appendix. A.

Table 1: Categorization of included methods. LiGAN, 3DSBDD and VOXBIND model atom positions as discrete variables; One-shot methods maintain a constant atom number in a generation, like diffusion-based ones; FLAG and D3FG use fragment motifs, and DECOMPDIFF uses arm&scaffolding priors.

Method	Continuous Position	One-shot Generation	Domain Knowledge
LiGAN	✗	✓	✗
3DSBDD	✗	✗	✗
POCKET2MOL	✓	✗	✗
GRAPHBP	✓	✗	✗
TARGETDIFF	✓	✓	✗
DIFFBP	✓	✓	✗
DIFFSBDD	✓	✓	✗
FLAG	✓	✗	✓
D3FG	✓	✓	✓
DECOMPDIFF	✓	✓	✓
MOLCRAFT	✓	✓	✗
VOXBIND	✗	✓	✗

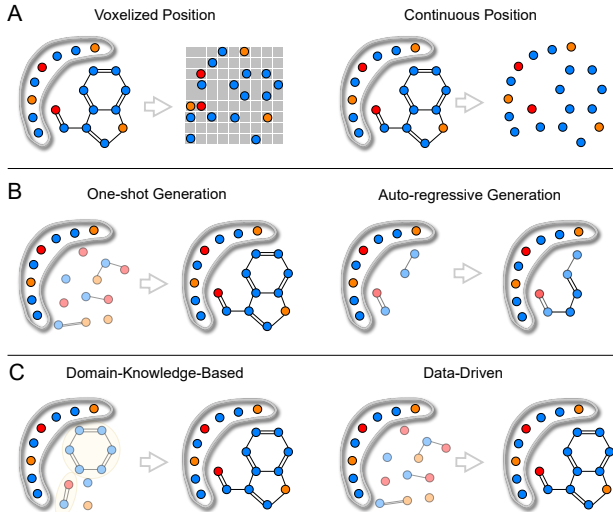


Figure 2: The demonstration of the classification criteria for the existing methods. The gray thick curves outline the contact surface of the protein, and the circles represent different types of atoms.

3 TASK AND DATASET

For the *de novo* molecule generation, we follow the previous protocol to use Crossdocked2020 (Francoeur et al., 2020) and data preparation with splits proposed in LiGAN (Masuda et al., 2020) and 3DSBDD (Luo et al., 2022) as the training and test sets. Besides the *de novo* generation, the modularized methods can be extended to four subtasks which are branches of our defined fill-in-the-blank of the complex binding graph, including the target-aware linker, fragment, side chain, and scaffold design (Zhang et al., 2024), leading to the generative targets \mathcal{G} for the probabilistic model $p(\mathcal{G}|\mathcal{C}, \mathcal{P})$ to be the four components, and the molecular context \mathcal{C} as the rest, as shown in Figure. 3. We demonstrate the significance of the four tasks in lead optimization and how the corresponding datasets are established below. The datasets are all established based on previous splits of Crossdocked2020 for a fair comparison.

Linker Design is a critical strategy in fragment-based drug discovery (Grenier et al., 2023). It focuses on creating linkers that connect two lead fragments and obtaining a complete molecule with enhanced affinity. Effective linker design can significantly influence the efficacy and pharmacokinetics of the drug, by ensuring that the molecule maintains the desired orientation and conformation when bound to its target (Erlanson et al., 2016). We define linkers following specific rules: (i) A linker should act as the intermediate structure connecting two fragments. (ii) A linker should contain at least two atoms on the shortest path between two fragments. (iii) Each connecting fragment must consist of more than five atoms.

Fragment Growing focus on expanding a fragment on the lead compound to better fill the binding pocket (Bancet et al., 2020). It also relates to adjusting pharmacological properties, such as enhancing solubility or reducing toxicity (Hung et al., 2009). We decompose the entire ligand into two fragments and select the smaller one for expansion based on specific criteria: (i) Each fragment must contain more than five atoms. (ii) The smaller fragment should be larger than half the size of the larger one.

Side Chain Decoration differs from fragment growing in that it permits modifications at multiple sites on the lead compound, whereas fragment growing typically modifies a single site. The taxonomy of arms-scaffold in previous work (Guan et al., 2024) is similar to side-chain-scaffold, while we focus on a chemist-intuitive approach, Bemis-Murko decomposition (Bemis & Murcko, 1996), which treats all terminal non-cyclic structures as side chains.

Scaffold Hopping is introduced by Schneider et al. (1999), as a strategy in medicinal chemistry aiming to replace the core structure of molecules to explore more diverse chemical space or improve

Table 2: The instance number of training and test split in the datasets for the four tasks and *De novo* generation. The decomposition is conducted separately in the training and test set of Cross-Docked2020 to avoid label leakage. Side chain decoration and scaffold hopping are two dual tasks, so the training and test set numbers are the same.

Dataset	# Training	# Test
<i>De novo</i>	99900	100
Linker	52685	43
Fragment	61379	61
Side Chain	70617	64
Scaffold	70617	64

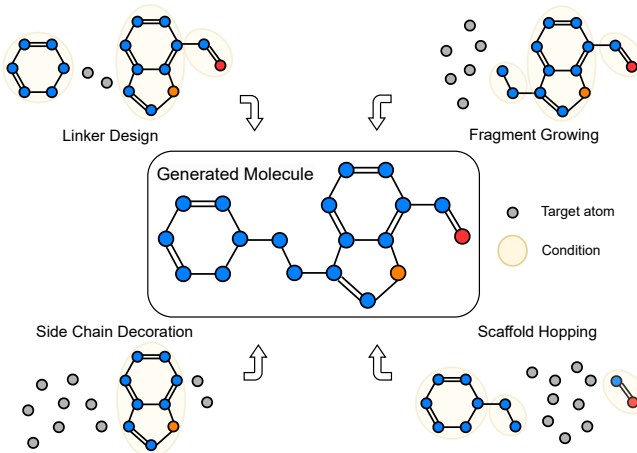


Figure 3: Demonstration of the four tasks.

specific properties. While various empirical definitions exist (Sun et al., 2012), for consistency, the Bemis-Murko decomposition is utilized to define the scaffold structure.

Since chances are that there is no substructure in a molecule according to the discussed definition of the decomposition, we here give the instance number of training and test set for each task in Table. 2.

4 EVALUATION PROTOCOL

In previous works, the evaluation usually focuses on two aspects including **interaction** and **chemical property**. While lots of works start to focus another two standards on molecule 3D structure’s authenticity with **geometry** analysis and the 2D graphs reliability with **substructure** analysis, the evaluation protocol is usually not unified. In this way, we extend them in a unified protocol including the four aspects as the following:

Substructure. To evaluate whether the model succeeds in learning the 2D graph structures for drug molecules. We expand previous metrics to functional groups, as certain functional groups in the drugs act as pharmacophores, such as phenol and pyrimidine. We identify the 25 most frequently occurring functional groups by using EFG (Salmina et al., 2015) (Appendix. B.1 gives the details), and calculated mean frequency of each function group generated in a molecule and the overall multinomial distribution. In the same way, the two values can also be obtained according to rings and atom types. The generated frequency and distribution against the references lead to 6 metrics on substructure analysis including the Jensen-Shannon divergence as JSD and mean absolute error as MAE, listed as (i) $JSD_{at}(\downarrow)$, (ii) $MAE_{at}(\downarrow)$, (iii) $JSD_{rt}(\downarrow)$, (iv) $MAE_{rt}(\downarrow)$, (v) $JSD_{fg}(\downarrow)$, and (vi) $MAE_{fg}(\downarrow)$, where ‘at’ means atom type, ‘rt’ means ring type and ‘fg’ means functional group.

Chemical Property. We continue the evaluation of chemical properties from most previous works, including (i) **QED**(\uparrow) as quantitative estimation of drug-likeness; (ii) **SA**(\uparrow) as synthetic accessibility score; (iii) **LogP** represents the octanol-water partition coefficient, and in general LogP values should be between -0.4 and 5.6 to be good drug candidates (Ghose et al., 1999); (iv) **LPSK**(\uparrow) as the ratio of the generated drug molecules satisfying the Lipinski’s rule of five.

Interaction. In evaluating the generated molecules’ interaction with proteins, the binding affinity is usually the most important metric. Here we unify the affinity calculation with AutoDock Vina for fair comparison. However, previous studies show that larger molecule sizes will lead to a higher probability that the generated molecules can interact with the protein, resulting in higher predicted binding affinity (Abad-Zapatero & Metz, 2005; Hopkins et al., 2014a). It is also an observation in this paper as the Pearson correlation of Vina Energy v.s. atom number reaches -0.67 (See Appendix. B.2). Besides, in some structures, there are more atoms in the protein participating in the interaction, which also causes the average to be unreasonable. Therefore, besides the commonly-used (i) $E_{vina}(\downarrow)$ as the mean Vina Energy, and (ii) **IMP**%(\uparrow) as the improvements indicating the ratio of the generated molecule with lower binding energy than the reference, we use mean percent binding gap as (iii) **MPBG**(\uparrow) (Appendix. B.3 gives computation) and ligand binding efficacy as (iv) **LBE**(\uparrow), written

as $\text{LBE}_i = -\frac{E_{\text{vina}}}{N_{\text{lig}}}$, indicating how much does a single atom in the molecule contribute to the binding affinity, to eliminate the effects of molecule sizes. We give a detailed discussion on the reasonability of LBE in Appendix. B.4. Moreover, it is important for the generated molecules to keep the same or similar interaction patterns with proteins (Zhang et al., 2023a). Therefore, we aim to figure out whether the SBDD models can learn the microscopic interaction patterns hidden in the data of the 3D conformations. We use PLIP (Adasme et al., 2021; Li Zuo et al., 2023; Salentin et al., 2015) to characterize the 7 types of interactions and calculate per-pocket and overall JSD between the categorical distributions of generated types and reference types and MAE between the frequency of each generated types v.s. it of reference types, in which the frequency is defined as the average number of occurrences of each type of interaction produced by different single generated molecules binding to the same protein, leading to four metrics including (v) $\text{JSD}_{\text{PP}}(\downarrow)$, (vi) $\text{JSD}_{\text{OA}}(\downarrow)$, (vii) $\text{MAE}_{\text{PP}}(\downarrow)$, (viii) $\text{MAE}_{\text{OA}}(\downarrow)$, where ‘PP’ and ‘OA’ means per-pocket and overall respectively.

Geometry. The internal geometry is an important characteristic for distinguishing between general point clouds and molecular structures. The torsion angles (Jing et al., 2022; Swanson et al., 2023) are flexible geometries, while bond lengths and bond angles are static to reveal whether the generated molecules have realistic structures. Hence, we evaluate the overall JSD of bond length and angle distribution between reference and generated ones, written as (i) $\text{JSD}_{\text{BL}}(\downarrow)$ and (ii) $\text{JSD}_{\text{BA}}(\downarrow)$. The other perspective for validating structural reasonability is the clash, the occurrence of which is defined when the van der Waals radii overlap by $\geq 0.4\text{\AA}$ (Ramachandran et al., 2011). Hence, the ratio of number of atoms generating clashes with protein atoms to the total atom number is written as (iii) $\text{Ratio}_{\text{cca}}(\downarrow)$ (cross clashes at atom level). Besides, the ratio of molecules with clashes as (iv) $\text{Ratio}_{\text{cm}}(\downarrow)$ (molecule with clashes) are evaluated.

We here evaluate the 12 methods discussed in Table. 1, and use Friedman rank (Friedman, 1940; 1937; Wang et al., 2022) as the mean ranking method, to fairly compare the performance of different models in the four aspects. The ranking score is calculated by $(12 - \text{rank})$, and the final rank is according to the weighted mean ranking score. Appendix. B.3 gives detailed computation of the metrics, and their explanations as preliminary. The review of each method’s evaluation aspect in the published papers is given in Appendix. B.5.

5 BENCHMARK RESULT

5.1 De novo GENERATION

5.1.1 SETUP

Training. We use the default configuration in each model’s released codebase as the hyperparameter, and set the training iteration number as 5,000,000 for fair comparison. It is noted that the loss of autoregressive methods exhibits a faster convergence rate of loss, typically requiring only a few tens of thousands of epochs to reach the final best checkpoint. To eliminate the effect brought about by the architecture of GNNs, in implementation, we use GVP (Jing et al., 2020) and EGNN (Satorras et al., 2022) with GAT (Veličković et al., 2018), as message-passing modules of auto-regressive and diffusion-based models, respectively. Especially, the GNN for encoding and decoding functional groups in D3FG is a combination of GAT and LoCS (Kofinas et al., 2022), CNN for processing atom density maps is four convolution blocks in LiGAN, and larger-scaled UNet for VOXBIND. The details in hyperparameter tuning and training strategy are given in Appendix. D.

Evaluation. Following the previous protocol, we generate 100 molecules per pocket in the test set, while not all the generated molecules are chemically valid (See Appendix. E.4), which will lead to <10,000 molecules. In affinity evaluation, we employ three modes of AutoDock Vina, including ‘Score’, ‘Minimize’, and ‘Dock’. MPBG and LBE are added to the Vina Dock mode. For Vina energy that is larger than 0, we think it is invalid, so we will not report it, and give the lowest ranking in the column of metrics. Moreover, LogP only provides a reference range for drug molecules, so we assigned a rank of 1 to the generated molecules within the rank of 2 to those outside the range. In all the tables, values in **bold** are the best metric, and values with underline are the second and third.

5.1.2 RESULT ANALYSIS

Substructure. Table. 3 gives results on 2D substructures, showing that (i) Overall, the auto-regressive models perform worse than the one-shot ones, especially in ring-type evaluation, where the

Table 3: Results of substructure analysis.

Methods	Metrics		Atom type		Ring type		Functional Group		Rank
	JSD _{at}	MAE _{at}	JSD _{rt}	MAE _{rt}	JSD _{fg}	MAE _{fg}			
LIGAN	0.1167	0.8680	0.3163	0.2701	0.2468	<u>0.0378</u>	6.33		
3DSBDD	0.0860	0.8444	0.3188	0.2457	0.2682	0.0494	6.33		
GRAPHBP	0.1642	1.2266	0.5061	0.4382	0.6259	0.0705	11.17		
POCKET2MOL	0.0916	1.0497	0.3550	0.3545	0.2961	0.0622	8.33		
TARGETDIFF	0.0533	0.2399	<u>0.2345</u>	0.1559	0.2876	<u>0.0441</u>	<u>3.33</u>		
DIFFSBDD	<u>0.0529</u>	0.6316	0.3853	0.3437	0.5520	0.0710	8.16		
DIFFBP	0.2591	1.5491	0.4531	0.4068	0.5346	0.0670	10.67		
FLAG	0.1032	1.7665	0.2432	0.3370	0.3634	0.0666	8.50		
D3FG	0.0644	0.8154	0.1869	0.2204	0.2511	0.0516	4.67		
DECOMPDIFF	0.0431	<u>0.3197</u>	0.2431	0.2006	<u>0.1916</u>	0.0318	2.50		
MOLCRAFT	<u>0.0490</u>	<u>0.3208</u>	0.2469	0.0264	<u>0.1196</u>	0.0477	<u>3.00</u>		
VOXBIND	0.0942	0.3564	<u>0.2401</u>	<u>0.0301</u>	0.1053	0.0761	5.00		

Table 4: Results of chemical property.

	QED	LogP	SA	LPSK	Rank
LIGAN	0.46	0.56	0.66	4.39	4.75
3DSBDD	0.48	0.47	0.63	4.72	3.50
GRAPHBP	0.44	3.29	0.64	4.73	3.75
POCKET2MOL	0.39	2.39	0.65	4.58	4.75
TARGETDIFF	0.49	1.13	0.60	4.57	4.25
DIFFSBDD	0.49	-0.15	0.34	4.89	3.50
DIFFBP	0.47	5.27	0.59	4.47	5.25
FLAG	0.41	0.29	0.58	4.93	4.25
D3FG	0.49	1.56	0.66	4.84	2.00
DECOMPDIF	0.49	1.22	0.66	4.40	3.75
MOLCRAFT	0.48	0.87	0.66	4.39	4.00
VOXBIND	0.54	2.22	0.65	4.70	2.75

Table 5: Results of interacton analysis.

Methods	Metrics		Vina Score		Vina Min		Vina Dock				PLIP Interaction				Rank
	E_{vina}	IMP%	E_{vina}	IMP%	E_{vina}	IMP%	MPBG%	LBE	JSD _{OA}	MAE _{OA}	JSD _{PP}	MAE _{PP}			
LIGAN	-6.47	62.13	-7.14	70.18	-7.70	72.71	4.22	0.3897	0.0346	0.0905	0.1451	0.3416	2.91		
3DSBDD	-	3.99	-3.75	17.98	-6.45	31.46	9.18	0.3839	0.0392	0.0934	0.1733	0.4231	7.17		
GRAPHBP	-	0.00	-	1.67	-4.57	10.86	-30.03	0.3200	0.0462	0.1625	0.2101	0.4835	11.33		
POCKET2MOL	-5.23	31.06	-6.03	38.04	-7.05	48.07	-0.17	0.4115	0.0319	0.2455	0.1535	0.4152	5.67		
TARGETDIFF	-5.71	38.21	-6.43	47.09	-7.41	51.99	5.38	0.3537	0.0198	0.0600	0.1757	0.4687	4.67		
DIFFSBDD	-	12.67	-2.15	22.24	-5.53	29.76	-23.51	0.2920	0.0333	0.1461	0.1777	0.5265	9.25		
DIFFBP	-	8.60	-	19.68	-7.34	49.24	6.23	0.3481	0.0249	0.1430	0.1256	0.5639	7.41		
FLAG	-	0.04	-	3.44	-3.65	11.78	-47.64	0.3319	0.0170	0.0277	0.2762	0.3976	9.00		
D3FG	-	3.70	-2.59	11.13	-6.78	28.90	-8.85	0.4009	0.0638	0.0135	0.1850	0.4641	8.17		
DECOMPDIF	-5.18	19.66	-6.04	34.84	-7.10	48.31	-1.59	0.3460	0.0215	0.0769	0.1848	0.4369	6.08		
MOLCRAFT	-6.15	54.25	-6.99	56.43	-7.79	56.22	8.38	0.3638	0.0214	0.0780	0.1868	0.4574	3.75		
VOXBIND	-6.16	41.80	-6.82	50.02	-7.68	52.91	9.89	0.3588	0.0257	0.0533	0.1850	0.4606	4.00		

former ones are more likely to generate triangular and tetrahedral rings. (ii) Diffusion-based models also exhibit advantages in atom type, according to the results of TARGETDIFF and MOLCRAFT, except for DIFFBP has difficulties in generating atoms with low occurrence frequencies. (iii) Besides VOXBIND, MOLCRAFT shows the overall superiority in complex functional group generation, as it states in addressing the mode collapse issues, while DECOMPDIF and D3FG also exhibit advantages due to the incorporation of prior knowledge in ring types and functional groups. DIFFBP and DIFFSBDD perform poorly due to inconsistencies in generating complex fragments. For a detailed comparison, see Appendix. E.1.1

Chemical Property. The chemical property is calculated with 2D molecule graphs, so it can be greatly influenced by the molecule substructures. From Table. 4, we can conclude that (i) In terms of the four metrics, the differences among the compared methods are not significant. (ii) D3FG shows the best overall properties, with the competitive QED, SA, and LPSK.

Interaction. From Table. 5 shows that (i) LIGAN and VOXBIND as CNN-based methods generate molecules that are initialized with high stability according to its competitive performance in Vina Score and Vina Min. It also performs well in Vina Dock mode, with a positive MPBG and high LBE, providing good consistency in interaction patterns. (ii) Auto-regressive methods except POCKET2MOL can hardly capture the pocket conditions and generate stably-binding molecules well, with very low IMP% in all Vina modes, while POCKET2MOL is the state-of-the-art auto-regressive method in *de novo* generation. (iii) In diffusion-based methods, MOLCRAFT outperform the other competitors in overall interaction comparison, and TARGETDIFF and DECOMPDIF perform competitively since the difference between these two methods is minimal. DIFFBP’s performance in docking mode is comparable, but in other modes, it performs less satisfactorily. Performance of DIFFSBDD is less than satisfactory. D3FG generates molecules with comparable Vina Energy but small atom numbers, leading to high LBE. For details, see Appendix. E.1.2.

Geometry. From Table. 6, conclusions can be drawn that (i) MOLCRAFT generates overall the most realistic structures, according to the internal geometries, and DECOMPDIF is comparable. (ii) The molecule-protein clashes can usually be avoided by diffusion-based models. However, in the auto-regressive models, only POCKET2MOL avoids clashes. The high frequency of clashes in auto-regressive methods can be explained as follows: These models first identify frontier amino acids or atoms within the molecule. During the placing of new atoms, incorrect binding site localization leads to an erroneous direction for the molecule’s auto-regressively growing path, causing it to extend inward towards the protein. For detailed results, see Appendix. E.1.3.

Table 6: Results of geometry analysis.

Methods	Metrics		Static Geometry		Clash		Rank
	JSD _{BL}	JSD _{BA}	Ratio _{cca}	Ratio _{cm}			
LiGAN	0.4645	0.5673	0.0096	0.0718	5.75		
3DSBDD	0.5024	0.3904	0.2482	0.8683	8.75		
GRAPHBP	0.5182	0.5645	0.8634	0.9974	11.50		
POCKET2MOL	0.5433	0.4922	0.0576	0.4499	8.50		
TARGETDIFF	<u>0.2659</u>	<u>0.3769</u>	0.0483	0.4920	4.50		
DIFFSBDD	0.3501	0.4588	0.1083	0.6578	7.25		
DIFFBP	0.3453	0.4621	0.0449	0.4077	5.25		
FLAG	0.4215	0.4304	0.6777	0.9769	9.00		
D3FG	0.3727	0.4700	0.2115	0.8571	8.50		
DECOMPDIFF	0.2576	0.3473	0.0462	0.5248	<u>4.00</u>		
MOLCRAFT	0.2250	0.2683	<u>0.0264</u>	<u>0.2691</u>	2.00		
VOXBIND	0.2701	0.3771	<u>0.0103</u>	<u>0.1890</u>	<u>3.00</u>		

Table 7: Ranking scores and overall ranking.

Methods	Weights	Substruc.	Chem.	Interact.	Geom.	Rank
	0.2	0.2	0.4	0.2	0.2	
LiGAN	1.13	1.45	3.63	1.25	<u>3</u>	
3DSBDD	1.13	1.70	1.93	0.65	7	
GRAPHBP	0.17	1.65	0.27	0.10	12	
POCKET2MOL	0.73	1.45	2.53	0.70	7	
TARGETDIFF	1.73	1.55	2.93	1.50	<u>2</u>	
DIFFSBDD	0.77	1.70	1.10	0.95	10	
DIFFBP	0.27	1.35	1.83	1.35	9	
FLAG	0.70	1.55	1.20	0.60	11	
D3FG	1.47	2.00	1.53	0.70	6	
DECOMPDIFF	1.90	1.65	2.57	1.60	4	
MOLCRAFT	1.80	1.60	3.30	2.00	1	
VOXBIND	1.40	1.85	3.20	1.80	5	

Conclusion and Discussion. From Table. 7 and the previous discussion, we conclude that

- (i) The CNN-based methods like LiGAN and VOXBIND are highly competitive, especially in aspects of **Interaction**, which explains why such methods in the field of drug design and molecule generation still prevail in recent years. This is partly attributed to *the fact that CNNs have an advantage over GNNs in perceiving many-body patterns within a single filter* (Townshend et al., 2021). As a result, it encourages further research into GNNs for 3D point clouds to develop architectures that can match the expressivity of CNNs.
- (ii) MOLCRAFT achieves the best overall performance, with TARGETDIFF closely following. In contrast, DECOMPDIFF and D3FG as the variants of TARGETDIFF that incorporate domain knowledge show some degeneration in performance. This observation reveals that the current incorporation of physicochemical priors can hardly improve the quality of generated molecules. *Effectively integrating domain knowledge to guide the model to generate structurally sound molecules remains a challenge.* For example, atom clashes are very common in generated molecules. While DECOMPDIFF employs the prior guidance for this, the problem has still not been fully solved. Integrating domain knowledge into the training process may mitigate this issue (Huang et al., 2024a; Adams & Coley, 2023).
- (iii) Only POCKET2MOL as an auto-regressive method achieves competitive results, which we attribute to the following reasons: First, it utilizes chemical bonds to constrain atoms to grow orderly along chemical bonds rather than to grow based on distance to the pocket as in DIFFBP. Second, it simultaneously predicts the bond types and employs contrastive learning by sampling positive and negative instances of atom positions as real and fake bonds, which is not fully considered by FLAG, enhancing the model’s ability to perceive chemical bond patterns. Therefore, we believe that *enabling the autoregressive methods model to successfully capture the patterns of chemical bonds is very essential.*

5.2 EXTENSION ON SUBTASKS

Setup. Lead optimization is to strengthen the function or property of the binding molecules by remodeling the existing partial 3D graph of molecules. We show the interaction analysis and chemical property in the main context and omit the interaction pattern analysis since maintaining the patterns is not necessary for lead optimization. The domain-knowledge-based methods can hardly be transferred for these tasks since different tasks require different priors, so we have not compared them here. Besides, the voxelize-based methods are not easily extended to these tasks, and we regard the transferring of methods like LiGAN and 3DSBDD as future work. Hence, we here compare 6 methods that model atoms’ continuous positions with GNNs and have not employed domain knowledge. When training, since the number of training instances is smaller, we use the pretrained models on *de novo* generation and finetune the auto-regressive models with 1,000,000 iterations. For diffusion-based models with one-shot generation, we train them from scratch because the zero-center-of-mass (Satorras et al., 2021) technique is shifted from employing protein geometric centers to using molecule context’s ones. For detailed results, please refer to Appendix. E.2.

Conclusion and Discussion. From Table. 8 and the previous discussion, we conclude that

- (i) Overall, the performance gap among these methods in the lead optimization is not as pronounced compared to *de novo* generation. MOLCRAFT, TARGET and POCKET2MOL maintain the good performance. Notably, in the evaluation of the stability of initial poses, the

other three also complete the binding graph near the given partial molecular conformations well, according to the columns of Vina Score and Vina Min. The applicability of GRAPHBP also reflects the *Argument. (ii)* in our *de novo* geometry analysis: The failure of GraphBP mainly stems from the difficulty in locating the correct atoms for auto-regressive growth.

- (ii) In these tasks, scaffold hopping is the most challenging task, as the improvement of generated molecules relative to the reference is minimal; Linker design is relatively the easiest. Notably, in scaffolding, there are still some methods that fail.
- (iii) There is a large space for improvements in these tasks, since the MPBG% metrics are usually negative, indicating that in most cases, the molecule is not optimized. Some edge-cutting techniques such as DPO (Rafailov et al., 2024; Cheng et al., 2024; Gu et al., 2024) and ITA (Yang et al., 2020; Kong et al., 2023; Lin et al., 2024) may be used to augment the optimized molecules as supervision signals for the models.

Additionally, several points warrant further detailed design. For instance, in linker design, the fragments of the molecule that need to be connected may change orientation due to variations in the linker (Guan et al., 2023a); In side chain decoration, the protein’s side chains, which are the main components in interaction, should be generated together with the molecule’s side chains to achieve a stable conformation as the entire complex (Luo et al., 2023; Huang et al., 2024b).

5.3 CASE STUDY ON REAL-WORLD TARGETS

Introduction. In order to verify whether the included methods can generalize to pharmaceutical targets and the applicability of CBGBench to real-world scenarios, we use the pretrained model in *de novo* generation, and apply them to two proteins belonging to the G-Protein-Coupled Receptor (GPCR) family: ARDB1 (beta-1 adrenergic receptor) and DRD3 (dopamine receptor D3). ARDB1 participates in the regulation of various physiological processes by responding to the neurotransmitter epinephrine (adrenaline) and norepinephrine, and drugs that selectively activate or block this receptor are used in the treatment of various cardiovascular conditions. For DRD3, it is primarily expressed in the brain, particularly in areas such as the limbic system and the ventral striatum with functions of mediating the effects of the neurotransmitter dopamine in the central nervous system.

Setup. On these targets, there are molecules reported active to them experimentally, we here randomly select 200 of them for each target and conduct two kinds of experiments. Firstly, we try to figure out if the model can generate binding molecules that have similar chemical distributions with the actives. We use extended connectivity fingerprint (ECFP) (Rogers & Hahn, 2010) to get the molecule fingerprint and employ t-SNE (van der Maaten & Hinton, 2008) for 2-dimensional visualization. Secondly, we aim to find out the distribution of Vina Docking Energy and LBE of the generated and the actives as the metrics for binding affinities. Eight methods except for voxelized-based ones (inflexible to extend) and DECOMPDIF (requiring complex data-preprocessing for domain knowledge) are tested on the two targets. Besides, we select 100 molecules randomly from GEOM-DRUG (Axelrod & Gómez-Bombarelli, 2022), as a randomized control sample set.

Conclusion and Discussion. Figure. 4 and Figure. 5 gives the results on target ADRB1.

- (i) In Figure. 4, we can see that POCKET2MOL, TARGETDIFF, D3FG, and MOLCRAFT have better consistency in the chemical distribution of molecules, as evidenced by a greater degree of overlap with the actives. In addition, in comparison to randomly selected molecules in GEOM-DRUG, these models show different preferences in generating binding molecules since the clustering center in the chemical space differs.
- (ii) Figure. 5 shows that in generating molecules based on the real-world target ADRB1, D3FG exhibits superior performance. TARGETDIFF and MOLCRAFT perform comparably.

These conclusions are essentially consistent with the conclusion in Sec. 5.1, reflecting that the established evaluation protocols exhibit **strong consistency and generalizability on real-world target data**. Besides, it is worth noting that DIFFBP, GRAPHBP, and POCKET2MOL can possibly generate molecules with small atom numbers and high LBE. This indicates that they have the potential to excel in lead discovery on ADRB1, as a good lead should possess good synthesizability and modifiability, smaller molecular weight, and stable binding conformations. For DRD3, please refer to Appendix. E.3 for details.

Table 8: Results of subtasks for lead optimization.

Tasks	Methods	Metrics		Vina Score		Vina Min		Vina Dock				Chem. Prop.				Rank
		E_{vina}	IMP%	E_{vina}	IMP%	E_{vina}	IMP%	MPBG%	LBE	QED	LogP	SA	LPSK			
Linker	GRAPHBP	-	5.63	-0.97	12.43	-7.51	28.18	-7.36	0.3288	0.41	0.86	0.70	3.60	4.75		
	POCKET2MOL	-6.89	18.99	-7.19	25.04	-8.07	37.22	-3.85	0.3276	0.45	1.93	0.67	4.25	2.83		
	TARGETDIFF	-7.22	36.11	-7.60	41.31	-8.49	50.73	2.61	0.2993	0.39	1.63	0.61	4.02	3.17		
	DIFFSBDD	-5.64	11.06	-6.38	19.15	-7.88	34.97	-4.42	0.3110	0.42	1.14	0.66	4.10	4.25		
	DIFFBP	-6.27	35.49	-7.19	36.80	-8.74	54.33	6.60	0.3078	0.43	3.45	0.55	4.01	3.25		
	MOLCRAFT	-7.13	38.80	-7.81	42.56	-8.81	58.44	5.09	0.3334	0.43	1.06	0.67	4.14	1.50		
Fragment	GRAPHBP	-5.54	4.86	-6.28	9.78	-7.16	16.21	-11.88	0.3749	0.54	0.87	0.66	4.66	3.58		
	POCKET2MOL	-6.87	22.78	-7.61	37.45	-8.33	54.05	-0.28	0.3310	0.46	1.02	0.63	4.07	2.00		
	TARGETDIFF	-6.06	24.56	-6.78	30.43	-7.96	42.00	-2.38	0.3003	0.45	1.43	0.58	4.28	3.33		
	DIFFSBDD	-4.64	19.14	-5.84	28.90	-7.66	37.18	-6.67	0.3076	0.47	0.73	0.58	4.39	4.17		
	DIFFBP	-4.51	22.31	-6.18	29.52	-7.90	45.70	-1.92	0.2952	0.46	2.24	0.49	4.30	4.08		
	MOLCRAFT	-6.75	21.12	-7.06	36.07	-7.92	43.02	-0.09	0.3236	0.46	1.27	0.51	4.64	2.58		
Side chain	GRAPHBP	5.01	10.15	-5.43	11.46	-6.14	9.71	-11.05	0.4459	0.61	1.93	0.76	4.93	3.75		
	POCKET2MOL	-5.99	22.26	-6.56	33.29	-7.26	41.04	-4.34	0.3600	0.49	0.21	0.65	4.20	2.91		
	TARGETDIFF	-5.80	23.90	-6.50	35.81	-7.40	46.87	-2.55	0.3213	0.48	0.88	0.60	4.41	2.58		
	DIFFSBDD	-4.43	15.12	-5.99	30.23	-7.58	44.09	-9.38	0.3178	0.43	1.20	0.65	4.03	3.83		
	DIFFBP	-4.61	14.31	-5.73	24.29	-7.03	38.96	-7.38	0.3143	0.49	1.29	0.56	4.50	4.25		
	MOLCRAFT	-6.10	24.10	-6.64	35.58	-7.49	41.67	-3.12	0.3227	0.44	1.22	0.61	4.36	2.42		
Scaffold	GRAPHBP	-	0.00	-	0.06	-3.90	0.99	-50.62	0.3797	0.43	0.14	0.76	4.98	4.16		
	POCKET2MOL	-4.80	16.84	-5.71	23.08	-6.89	38.18	-8.07	0.3378	0.43	0.91	0.64	4.48	2.42		
	TARGETDIFF	-5.52	31.47	-5.86	34.39	-7.06	44.32	-6.22	0.3038	0.43	0.89	0.59	4.26	2.00		
	DIFFSBDD	-3.85	18.44	-4.90	22.12	-6.81	34.98	-10.23	0.2985	0.42	-0.13	0.53	4.29	4.17		
	DIFFBP	-2.09	13.89	-4.35	16.84	-6.46	32.43	-12.14	0.3025	0.43	3.37	0.56	4.44	4.17		
	MOLCRAFT	-4.71	14.03	-5.35	30.16	-7.02	43.53	-7.34	0.3146	0.42	1.01	0.56	4.55	2.83		

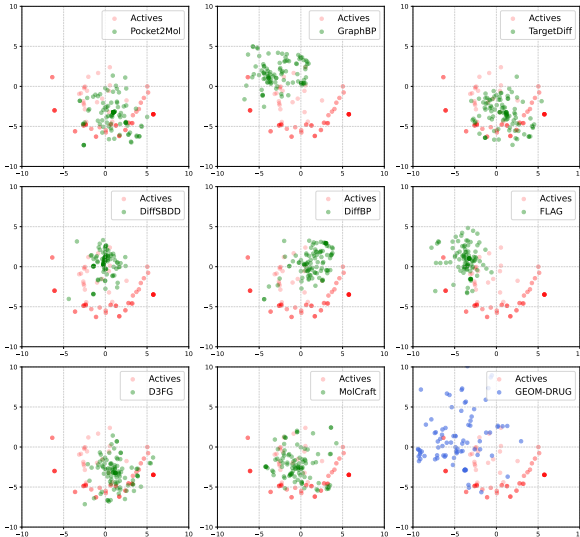
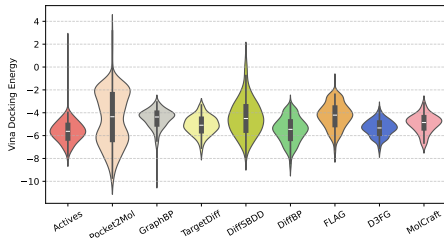
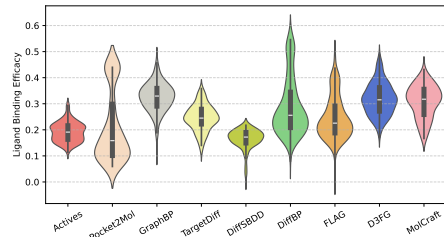


Figure 4: T-SNE visualization of chemical distributions of generated and active molecules on ADRB1.



(a) Distribution of Vina Dock Energy



(b) Distribution of LBE

Figure 5: Distribution of binding affinities.

6 CONCLUSION AND LIMITATION

In this paper, we propose CBGBench. It first unifies the tasks of SBDD and lead optimization into a 3D-graph completion problem as a fill-in-the-blank 3D binding graph and introduces four additional lead optimization tasks. Then, it comprehensively categorizes existing methods based on certain criteria, modularizes these methods based on the categorization, and integrates them into a unified codebase for fair comparison. Additionally, it extends existing evaluation protocols by incorporating aspects such as interaction pattern, ligand binding efficacy, and protein-atom clash ratio as important evaluation metrics, addressing the issue of incomplete and diverse evaluation process. Finally, through extensive experiments and by extending the pretrained models to real targets for molecule generation, we derive a series of insightful conclusions and identify future research directions.

However, there are certain limitations. Firstly, this codebase is primarily based on GNNs, so some voxelized-grid-based methods that require the use of CNNs have not been included. Engineering the integration of these types of methods will be a focus of our future work. Secondly, due to the inability to use wet lab experiments for validation, many of the metrics are obtained through

computational chemistry methods. These computational functions are often considered unable to accurately reflect the chemical properties of molecules, such as the calculated SA (Synthetic Accessibility) and AutoDock Vina Energy. Therefore, how to utilize AI to assist in accurate metric calculation will also be a key focus of our future research.

REFERENCES

- Cele Abad-Zapatero and James T Metz. Ligand efficiency indices as guideposts for drug discovery. *Drug discovery today*, 10(7):464–469, 2005.
- Keir Adams and Connor W. Coley. Equivariant shape-conditioned generation of 3d molecules for ligand-based drug design. In *The Eleventh International Conference on Learning Representations*, 2023. URL <https://openreview.net/forum?id=4MbGnp4iPQ>.
- Melissa F. Adasme, Katja L Linnemann, Sarah Naomi Bolz, Florian Kaiser, Sebastian Salentin, V. Joachim Haupt, and Michael Schroeder. Plip 2021: expanding the scope of the protein–ligand interaction profiler to dna and rna. *Nucleic Acids Research*, 49:W530 – W534, 2021.
- Simon Axelrod and Rafael Gómez-Bombarelli. Geom, energy-annotated molecular conformations for property prediction and molecular generation. *Scientific Data*, 9(1):185, 2022. doi: 10.1038/s41597-022-01288-4. URL <https://doi.org/10.1038/s41597-022-01288-4>.
- Alexandre Bancet, Claire Raingeval, Thierry Lomberget, Marc Le Borgne, Jean-François Guichou, and Isabelle Krimm. Fragment linking strategies for structure-based drug design. *Journal of Medicinal Chemistry*, 63(20):11420–11435, 2020.
- Guy W Bemis and Mark A Murcko. The properties of known drugs. 1. molecular frameworks. *Journal of medicinal chemistry*, 39(15):2887–2893, 1996.
- Xiwei Cheng, Xiangxin Zhou, Yuwei Yang, Yu Bao, and Quanquan Gu. Decomposed direct preference optimization for structure-based drug design, 2024. URL <https://arxiv.org/abs/2407.13981>.
- Daniel A Erlanson, Stephen W Fesik, Roderick E Hubbard, Wolfgang Jahnke, and Harren Jhoti. Twenty years on: the impact of fragments on drug discovery. *Nature reviews Drug discovery*, 15(9):605–619, 2016.
- Paul G. Francoeur, Tomohide Masuda, Jocelyn Sunseri, Andrew Jia, Richard B. Iovanisci, Ian Snyder, and David Ryan Koes. 3d convolutional neural networks and a crossdocked dataset for structure-based drug design. *Journal of chemical information and modeling*, 2020.
- Milton Friedman. The use of ranks to avoid the assumption of normality implicit in the analysis of variance. *Journal of the American Statistical Association*, 32:675–701, 1937.
- Milton Friedman. A comparison of alternative tests of significance for the problem of m rankings. *Annals of Mathematical Statistics*, 11:86–92, 1940.
- Arup K. Ghose, Vellarkad N. Viswanadhan, and John J. Wendoloski. A knowledge-based approach in designing combinatorial or medicinal chemistry libraries for drug discovery. 1. a qualitative and quantitative characterization of known drug databases. *Journal of combinatorial chemistry*, 1 1: 55–68, 1999.
- Alex Graves, Rupesh Kumar Srivastava, Timothy Atkinson, and Faustino Gomez. Bayesian flow networks, 2024. URL <https://arxiv.org/abs/2308.07037>.
- Dylan Grenier, Solène Audebert, Jordane Preto, Jean-François Guichou, and Isabelle Krimm. Linkers in fragment-based drug design: an overview of the literature. *Expert Opinion on Drug Discovery*, 18(9):987–1009, 2023.
- Siya Gu, Minkai Xu, Alexander Powers, Weili Nie, Tomas Geffner, Karsten Kreis, Jure Leskovec, Arash Vahdat, and Stefano Ermon. Aligning target-aware molecule diffusion models with exact energy optimization, 2024. URL <https://arxiv.org/abs/2407.01648>.

-
- Jiaqi Guan, Xingang Peng, Peiqi Jiang, Yunan Luo, Jian Peng, and Jianzhu Ma. Linkernet: Fragment poses and linker co-design with 3d equivariant diffusion. In *Neural Information Processing Systems*, 2023a.
- Jiaqi Guan, Wesley Wei Qian, Xingang Peng, Yufeng Su, Jian Peng, and Jianzhu Ma. 3d equivariant diffusion for target-aware molecule generation and affinity prediction. In *The Eleventh International Conference on Learning Representations*, 2023b. URL <https://openreview.net/forum?id=kJqXEPXMsEO>.
- Jiaqi Guan, Xiangxin Zhou, Yuwei Yang, Yu Bao, Jian Peng, Jianzhu Ma, Qiang Liu, Liang Wang, and Quanquan Gu. DecompDiff: Diffusion models with decomposed priors for structure-based drug design. In Andreas Krause, Emma Brunskill, Kyunghyun Cho, Barbara Engelhardt, Sivan Sabato, and Jonathan Scarlett (eds.), *Proceedings of the 40th International Conference on Machine Learning*, volume 202 of *Proceedings of Machine Learning Research*, pp. 11827–11846. PMLR, 23–29 Jul 2023c. URL <https://proceedings.mlr.press/v202/guan23a.html>.
- Jiaqi Guan, Xiangxin Zhou, Yuwei Yang, Yu Bao, Jian Peng, Jianzhu Ma, Qiang Liu, Liang Wang, and Quanquan Gu. Decompdiff: diffusion models with decomposed priors for structure-based drug design. *arXiv preprint arXiv:2403.07902*, 2024.
- Jonathan Ho, Ajay Jain, and P. Abbeel. Denoising diffusion probabilistic models. *ArXiv*, abs/2006.11239, 2020.
- Emiel Hoogeboom, Victor Garcia Satorras, Clément Vignac, and Max Welling. Equivariant diffusion for molecule generation in 3d, 2022. URL <https://arxiv.org/abs/2203.17003>.
- Andrew L Hopkins, György M Keserü, Paul D Leeson, David C Rees, and Charles H Reynolds. The role of ligand efficiency metrics in drug discovery. *Nature reviews Drug discovery*, 13(2):105–121, 2014a.
- Andrew L Hopkins, György M Keserü, Paul D Leeson, David C Rees, and Charles H Reynolds. The role of ligand efficiency metrics in drug discovery. *Nature Reviews Drug Discovery*, 13(2): 105–121, 2014b. doi: 10.1038/nrd4163.
- Lei Huang, Tingyang Xu, Yang Yu, Peilin Zhao, Xingjian Chen, Jing Han, Zhi Xie, Hailong Li, Wenge Zhong, Ka-Chun Wong, and Hengtong Zhang. A dual diffusion model enables 3d molecule generation and lead optimization based on target pockets. *Nature Communications*, 15, 2024a.
- Yufei Huang, Odin Zhang, Lirong Wu, Cheng Tan, Haitao Lin, Zhangyang Gao, Siyuan Li, and Stan. Z. Li. Re-dock: Towards flexible and realistic molecular docking with diffusion bridge, 2024b.
- Alvinemsp14W Hung, H emsp14Leonardo Silvestre, Shijun Wen, Alessio Ciulli, Tomemsp14L Blundell, and Chris Abell. Application of fragment growing and fragment linking to the discovery of inhibitors of mycobacterium tuberculosis pantothenate synthetase. *Angewandte Chemie International Edition*, 48(45):8452–8456, 2009.
- Ilia Igashov, Hannes Stärk, Clément Vignac, Victor Garcia Satorras, Pascal Frossard, Max Welling, Michael M. Bronstein, and Bruno E. Correia. Equivariant 3d-conditional diffusion models for molecular linker design. *ArXiv*, abs/2210.05274, 2022.
- Bowen Jing, Stephan Eismann, Patricia Suriana, Raphael J. L. Townshend, and Ron O. Dror. Learning from protein structure with geometric vector perceptrons. *ArXiv*, abs/2009.01411, 2020.
- Bowen Jing, Gabriele Corso, Jeffrey Chang, Regina Barzilay, and T. Jaakkola. Torsional diffusion for molecular conformer generation. *ArXiv*, abs/2206.01729, 2022.
- John M. Jumper, Richard Evans, Alexander Pritzel, Tim Green, Michael Figurnov, Olaf Ronneberger, Kathryn Tunyasuvunakool, Russ Bates, Augustin Židek, Anna Potapenko, Alex Bridgland, Clemens Meyer, Simon A A Kohl, Andy Ballard, Andrew Cowie, Bernardino Romera-Paredes, Stanislav Nikolov, Rishub Jain, Jonas Adler, Trevor Back, Stig Petersen, David Reiman, Ellen Clancy, Michal Zielinski, Martin Steinegger, Michalina Pacholska, Tamas Berghammer,

-
- Sebastian Bodenstein, David Silver, Oriol Vinyals, Andrew W. Senior, Koray Kavukcuoglu, Pushmeet Kohli, and Demis Hassabis. Highly accurate protein structure prediction with alphafold. *Nature*, 596:583 – 589, 2021.
- Peter W. Kenny. The nature of ligand efficiency. *Journal of Medicinal Chemistry*, 60(13):5583–5594, 2017. doi: 10.1021/acs.jmedchem.7b00074.
- Diederik P Kingma and Max Welling. Auto-encoding variational bayes, 2022.
- Miltiadis Kofinas, Naveen Shankar Nagaraja, and Efstratios Gavves. Roto-translated local coordinate frames for interacting dynamical systems, 2022.
- Xiangzhe Kong, Wenbing Huang, and Yang Liu. Conditional antibody design as 3d equivariant graph translation. In *The Eleventh International Conference on Learning Representations*, 2023. URL <https://openreview.net/forum?id=LFHFQbjxIiP>.
- Rohith Krishna, Jue Wang, Woody Ahern, Pascal Sturmfels, Preetham Venkatesh, Indrek Kalvet, Gyu Rie Lee, Felix S Morey-Burrows, Ivan V. Anishchenko, Ian R. Humphreys, Ryan McHugh, Dionne Vafeados, Xinting Li, George A. Sutherland, Andrew Hitchcock, C Neil Hunter, Alex Kang, Evans Brackenbrough, Asim K. Bera, Minkyung Baek, Frank DiMaio, and David Baker. Generalized biomolecular modeling and design with rosettafold all-atom. *bioRxiv*, 2023.
- Jia li Zuo, Changqian Yu, Nong Sang, and Changxin Gao. Plip: Language-image pre-training for person representation learning. *ArXiv*, abs/2305.08386, 2023.
- Haitao Lin, Yufei Huang, Meng Liu, Xuan Cindy Li, Shuiwang Ji, and Stan Z. Li. Diffbp: Generative diffusion of 3d molecules for target protein binding. *ArXiv*, abs/2211.11214, 2022.
- Haitao Lin, Yufei Huang, Haotian Zhang, Lirong Wu, Siyuan Li, Zhiyuan Chen, and Stan Z. Li. Functional-group-based diffusion for pocket-specific molecule generation and elaboration. *ArXiv*, abs/2306.13769, 2023.
- Haitao Lin, Lirong Wu, Yufei Huang, Yunfan Liu, Odin Zhang, Yuanqing Zhou, Rui Sun, and Stan Z. Li. GeoAB: Towards realistic antibody design and reliable affinity maturation. In *Forty-first International Conference on Machine Learning*, 2024. URL <https://openreview.net/forum?id=6pHP51F55x>.
- Yaron Lipman, Ricky T. Q. Chen, Heli Ben-Hamu, Maximilian Nickel, and Matt Le. Flow matching for generative modeling. *ArXiv*, abs/2210.02747, 2022.
- Meng Liu, Youzhi Luo, Kanji Uchino, Koji Maruhashi, and Shuiwang Ji. Generating 3d molecules for target protein binding. *ArXiv*, abs/2204.09410, 2022.
- Shitong Luo, Jiaqi Guan, Jianzhu Ma, and Jian Peng. A 3d generative model for structure-based drug design, 2022.
- Shitong Luo, Yufeng Su, Zuofan Wu, Chenpeng Su, Jian Peng, and Jianzhu Ma. Rotamer density estimator is an unsupervised learner of the effect of mutations on protein-protein interaction. In *The Eleventh International Conference on Learning Representations*, 2023. URL https://openreview.net/forum?id=_X9Y11K2mD.
- Tomohide Masuda, Matthew Ragoza, and David Ryan Koes. Generating 3d molecular structures conditional on a receptor binding site with deep generative models. *ArXiv*, abs/2010.14442, 2020.
- Andrew T. McNutt, Paul G. Francoeur, Rishal Aggarwal, Tomohide Masuda, Rocco Meli, Matthew Ragoza, Jocelyn Sunseri, and David Ryan Koes. Gnina 1.0: molecular docking with deep learning. *Journal of Cheminformatics*, 13, 2021.
- Christopher W Murray, Michael G Carr, Orla Callaghan, Gianluca Chessari, Miles Congreve, Steven Cowan, Paul Edwards, Mike Frederickson, Barry Graham, Rosemary McMenamin, Michelle A O’Brien, Susan Patel, Tim R Phillips, Gareth Williams, Alison J Woodhead, and Harren Jhoti. Fragment-based drug discovery applied to hsp90: Discovery of two lead series with high ligand efficiency. *Journal of Medicinal Chemistry*, 53(16):5942–5955, 2010. doi: 10.1021/jm1004102.

-
- Open Babel development team. Open babel. URL http://openbabel.org/wiki/Main_Page.
- Xingang Peng, Shitong Luo, Jiaqi Guan, Qi Xie, Jian Peng, and Jianzhu Ma. Pocket2mol: Efficient molecular sampling based on 3d protein pockets. In *International Conference on Machine Learning*, 2022.
- Pedro O. Pinheiro, Arian Jamasb, Omar Mahmood, Vishnu Sresht, and Saeed Saremi. Structure-based drug design by denoising voxel grids, 2024a.
- Pedro O. Pinheiro, Joshua Rackers, Joseph Kleinhenz, Michael Maser, Omar Mahmood, Andrew Martin Watkins, Stephen Ra, Vishnu Sresht, and Saeed Saremi. 3d molecule generation by denoising voxel grids, 2024b.
- Yanru Qu, Keyue Qiu, Yuxuan Song, Jingjing Gong, Jiawei Han, Mingyue Zheng, Hao Zhou, and Wei-Ying Ma. Molcraft: Structure-based drug design in continuous parameter space. *ICML 2024*, 2024.
- Rafael Rafailov, Archit Sharma, Eric Mitchell, Stefano Ermon, Christopher D. Manning, and Chelsea Finn. Direct preference optimization: Your language model is secretly a reward model, 2024. URL <https://arxiv.org/abs/2305.18290>.
- Srinivas Ramachandran, Pradeep Kota, Feng Ding, and Nikolay V. Dokholyan. Automated minimization of steric clashes in protein structures. *Proteins: Structure*, 79, 2011.
- RDKit, online. RDKit: Open-source cheminformatics. <http://www.rdkit.org>. [Online; accessed 11-April-2013].
- Charles Reynolds, Brett Tounge, and Scott Bembenek. Ligand binding efficiency: Trends, physical basis, and implications. *Journal of medicinal chemistry*, 51:2432–8, 05 2008. doi: 10.1021/jm701255b.
- David Rogers and Mathew Hahn. Extended-connectivity fingerprints. *Journal of chemical information and modeling*, 50 5:742–54, 2010.
- Sebastian Salentin, Sven Schreiber, V. Joachim Haupt, Melissa F. Adasme, and Michael Schroeder. Plip: fully automated protein–ligand interaction profiler. *Nucleic Acids Research*, 43:W443 – W447, 2015.
- Elena S. Salmina, Norbert Haider, and Igor V. Tetko. Extended functional groups (efg): An efficient set for chemical characterization and structure-activity relationship studies of chemical compounds. *Molecules*, 21, 2015.
- Victor Garcia Satorras, Emiel Hoogetboom, Fabian B. Fuchs, Ingmar Posner, and Max Welling. E(n) equivariant normalizing flows. In *Neural Information Processing Systems*, 2021.
- Victor Garcia Satorras, Emiel Hoogetboom, and Max Welling. E(n) equivariant graph neural networks, 2022.
- Gisbert Schneider, Werner Neidhart, Thomas Giller, and Gerard Schmid. “scaffold-hopping” by topological pharmacophore search: a contribution to virtual screening. *Angewandte Chemie International Edition*, 38(19):2894–2896, 1999.
- Arne Schneuing, Yuanqi Du, Charles Harris, Arian R. Jamasb, Ilia Igashov, Weitao Du, Tom L. Blundell, Pietro Li’o, Carla P. Gomes, Max Welling, Michael M. Bronstein, and Bruno E. Correia. Structure-based drug design with equivariant diffusion models. *ArXiv*, abs/2210.13695, 2022.
- Yang Song, Jascha Narain Sohl-Dickstein, Diederik P. Kingma, Abhishek Kumar, Stefano Ermon, and Ben Poole. Score-based generative modeling through stochastic differential equations. *ArXiv*, abs/2011.13456, 2020.
- Yuxuan Song, Jingjing Gong, Yanru Qu, Hao Zhou, Mingyue Zheng, Jingjing Liu, and Wei-Ying Ma. Unified generative modeling of 3d molecules via bayesian flow networks. *ICLR 2024*, 2024.

-
- Hongmao Sun, Gregory Tawa, and Anders Wallqvist. Classification of scaffold-hopping approaches. *Drug discovery today*, 17(7-8):310–324, 2012.
- Kirk Swanson, Jake Williams, and Eric Jonas. Von mises mixture distributions for molecular conformation generation, 2023.
- Raphael Townshend, Martin Vögele, Patricia Suriana, Alex Derry, Alexander Powers, Yianni Laloudakis, Sidhika Balachandar, Bowen Jing, Brandon Anderson, Stephan Eismann, Risi Kondor, Russ Altman, and Ron Dror. Atom3d: Tasks on molecules in three dimensions. In J. Vanschoren and S. Yeung (eds.), *Proceedings of the Neural Information Processing Systems Track on Datasets and Benchmarks*, volume 1, 2021. URL https://datasets-benchmarks-proceedings.neurips.cc/paper_files/paper/2021/file/c45147dee729311ef5b5c3003946c48f-Paper-round1.pdf.
- Oleg Trott and Arthur J. Olson. Autodock vina: Improving the speed and accuracy of docking with a new scoring function, efficient optimization, and multithreading. *Journal of Computational Chemistry*, 31, 2009.
- Laurens van der Maaten and Geoffrey E. Hinton. Visualizing data using t-sne. *Journal of Machine Learning Research*, 9:2579–2605, 2008.
- Petar Veličković, Guillem Cucurull, Arantxa Casanova, Adriana Romero, Pietro Liò, and Yoshua Bengio. Graph attention networks, 2018.
- Yidong Wang, Hao Chen, Yue Fan, Wangbin Sun, Ran Tao, Wenxin Hou, Renjie Wang, Linyi Yang, Zhi Zhou, Lan-Zhe Guo, Heli Qi, Zhen Wu, Yu-Feng Li, Satoshi Nakamura, Weirong Ye, Marios Savvides, Bhiksha Raj, Takahiro Shinozaki, Bernt Schiele, Jindong Wang, Xingxu Xie, and Yue Zhang. Usb: A unified semi-supervised learning benchmark. *ArXiv*, abs/2208.07204, 2022.
- Joseph L Watson, David Juergens, Nathaniel R. Bennett, Brian L. Trippe, Jason Yim, Helen E. Eisenach, Woody Ahern, Andrew J. Borst, Robert J. Ragotte, Lukas F. Milles, Basile I. M. Wicky, Nikita Hanikel, Samuel J. Pellock, Alexis Courbet, William Sheffler, Jue Wang, Preetham Venkatesh, Isaac Sappington, Susana Vázquez Torres, Anna Lauko, Valentin De Bortoli, Emile Mathieu, Sergey Ovchinnikov, Regina Barzilay, T. Jaakkola, Frank DiMaio, Minkyung Baek, and David Baker. De novo design of protein structure and function with rfdiffusion. *Nature*, 620:1089 – 1100, 2023.
- Kevin Yang, Wengong Jin, Kyle Swanson, Regina Barzilay, and Tommi Jaakkola. Improving molecular design by stochastic iterative target augmentation. In *International Conference on Machine Learning*, pp. 10716–10726. PMLR, 2020.
- Odin Zhang, Jintu Zhang, Jieyu Jin, Xujun Zhang, Renling Hu, Chao Shen, Hanqun Cao, Hongyan Du, Yu Kang, Yafeng Deng, Furui Liu, Guangyong Chen, Chang-Yu Hsieh, and Tingjun Hou. Resgen is a pocket-aware 3d molecular generation model based on parallel multiscale modelling. *Nature Machine Intelligence*, 5:1020 – 1030, 2023a.
- Odin Zhang, Haitao Lin, Hui Zhang, Huifeng Zhao, Yufei Huang, Yuansheng Huang, Dejun Jiang, Chang-yu Hsieh, Peichen Pan, and Tingjun Hou. Deep lead optimization: Leveraging generative ai for structural modification. *arXiv preprint arXiv:2404.19230*, 2024.
- Zaixi Zhang, Yaosen Min, Shuxin Zheng, and Qi Liu. Molecule generation for target protein binding with structural motifs. In *The Eleventh International Conference on Learning Representations*, 2023b. URL <https://openreview.net/forum?id=Rq13idF0F73>.

A REVIEW ON THE METHODS’ TIMELINE

Here we give a brief review of the 12 included methods in chronological order, with Table. ?? giving some standardized information on these methods.

- LiGAN is firstly proposed to incorporate a generative model for the SBDD task, in which the encoder and the decoder are 3-layer CNNs, and the Variational Auto-Encoder is employed to model the probability of the atom’s density map in a molecule. It split the training and test set in CrossDocked2020.
- Due to the rise of Graph Neural Networks (GNNs), 3DSBDD subsequently adopted GNNs for modeling this task. At that time, GNNs were more adept at handling pairwise information, so an autoregressive graph network modeling approach was chosen as an effective method for molecular modeling. However, the development of graph networks for 3D tasks remained slow, leading 3DSBDD to continue modeling molecules using voxelized maps. 3DSBDD leverages graph networks to predict the voxel position that the next atom will occupy, as well as the atom type, thereby generating molecules in an autoregressive manner. In addition, 3DSBDD further standardized the evaluation protocol of the experiment by using Vina Docking Energy to assess the stability of the generated molecules.
- The rise of EGNN has enabled autoregressive modeling of continuous atomic coordinates in the SBDD task while preserving equivariance and invariance properties. Following this development, GRAPHBP adopted the EGNN architecture, using a depth-first search approach to rank the molecules from near to far on the protein surface. This allows for autoregressive molecular generation starting from the protein frontier and ultimately modeling a complete molecule. However, GRAPHBP did not consider critical chemical priors such as bond lengths and bond angles between atoms, making it challenging to capture the internal patterns of molecules. The evaluation is based on Gnina Docking, different from 3DSBDD.
- Meanwhile, POCKET2MOL directly modeled atomic coordinates using GVP. Compared to GRAPHBP, POCKET2MOL took molecular bonds into account and employed contrastive learning, where false atoms were used to regularize the coordinates and bonding of real atoms. This significantly improved the stability of the generated molecules. The evaluation follows 3DSBDD.
- The rise of generative models, particularly the widespread application of diffusion models in the field of images, has drawn attention to these cutting-edge generative techniques in the molecular domain as well. Diffusion models are inspired by particle systems in statistical physics, which aligns closely with the task of generating atomic coordinates in molecules. DIFFSBDD, as pioneering works in applying diffusion models to the SBDD task, have also achieved significant results. DIFFSBDD followed most of the concepts from EDM, such as the zero-center-of-mass technique, and was tested and generalized on Binding MOAD beyond CrossDocked2020.
- Meanwhile, DIFFBP also proposed to use the Gaussian Diffusion model on atoms’ positions and masked type diffusion for elements’ types. DIFFBP analyzed the drawbacks of autoregressive models from the perspective of the Boltzmann energy distribution in statistical physics and observed that molecular weight severely affects docking performance, being the first to adopt a grouping approach for model comparison.
- After that, following previous explorations like GEODIFF and EDM in molecular (conformation) generation, TARGETDIFF innovatively introduced a diffusion model-based SBDD method, achieving new state-of-the-art (SOTA) performance. For validation, TARGETDIFF first proposed using Vina Score and Vina Min mode to assess the stability of the generated molecules’ initial states. Additionally, the embeddings learned by the model can also be used for affinity prediction.
- On the other hand, fragment-based generative methods are also in the early stages of exploration. FLAG follows the autoregressive generation approach of POCKET2MOL, breaking molecules into fragments and individual atoms, allowing for the generation of complex molecules with fewer steps. However, its modeling approach lacks sufficient consideration of chemical bond participation, which is a key reason for its suboptimal molecular generation performance.

- Afterward, D3FG combined fragment-based generation with the diffusion method, leveraging protein generation techniques to establish a diffusion model that predicts the orientation matrix, central coordinates, and fragment types based on fragment information. The model then uses linkers to connect the molecule fragments. Additionally, D3FG enables molecular optimization by replacing fragments that are either prominent or insufficiently contributing.
- In contrast to D3FG, which treats fragments as rigid bodies, DECOMPDIFF considers fragments as flexible structures, thereby decomposing molecules into arms and scaffolds, and performing multivariate Gaussian diffusion within different decomposition clusters. Additionally, DECOMPDIFF employs non-intersection guidance to mitigate the issue of atomic overlap between the molecule and protein amino acids.
- In addition, work on voxelized maps is steadily progressing. VOXBIND builds on the pioneering work of VOXMOL, using diffusion-based denoising modeling on the voxelized density map of molecules. During the generation steps, it incorporates wj-sampling to reduce computational complexity, while also producing structurally stable molecules.
- More recently, MOLCRAFT was proposed, utilizing the Bayes Flow Network, which is designed for modeling probabilistic densities’ parameters. This allows molecules to avoid the difficulty of coupling the two modalities: the discrete variable of atomic types and the continuous positions of atoms in the molecule. It effectively addresses issues such as mode collapse and has demonstrated outstanding performance as the most recent SOTA model.

Table 9: A brief review of the included methods.

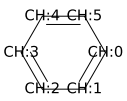
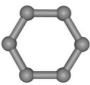
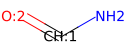
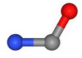
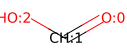
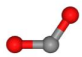
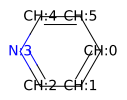
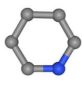
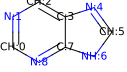
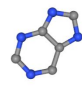

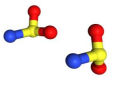
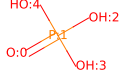

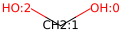
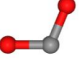
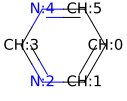
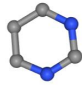
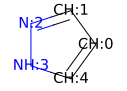
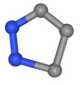
Method	Time	Generative Model	Network Structure	Prior Knowledge	Evaluation Datasets
LIGAN	Oct. 2020	VAE	CNN	None	CrossDocked2020
3DSBDD	Mar. 2022	Auto-regressive	GNN	None	CrossDocked2020
GRAPHBP	Apr. 2022	Auto-regressive	EGNN	None	CrossDocked2020
POCKET2MOL	May. 2022	Auto-regressive	GVP	None	CrossDocked2020
DIFFSBDD	Oct. 2022	DDPM	EGNN	None	CrossDocked2020 Binding MOAD
DIFFBP	Nov. 2022	DDPM	GVP	None	CrossDocked2020
TARGETDIFF	Feb. 2023	DDPM	EGNN	None	CrossDocked2020
FLAG	Feb. 2023	Auto-regressive	GVP	Fragment	CrossDocked2020
D3FG	May. 2023	DDPM	EGNN + IPA	Fragment	CrossDocked2020
DECOMPDIFF	Feb. 2024	DDPM	EGNN	Arm&Scaffold	CrossDocked2020
MOLCRAFT	Apr. 2024	BFN	EGNN	None	CrossDocked2020
VOXBIND	May. 2024	DDPM	CNN	None	CrossDocked2020

B SUPPLEMENTARY EVALUATION DETAILS

B.1 INCLUDED FUNCTIONAL GROUPS

Here we show the functional groups included in this paper, in which we follow D3FG and give a demonstration of them in Table. 10.

Table 10: The included functional groups in CBGBench. ‘T’ is the occurrence times of the functional group in the datasets (100,000 ligands). ‘A,B,C’ are the framing node index.

Smiles	2D graph	3D structures	A	B	C	T
c1ccccc1			1	0	2	131148
NC=O			1	0	2	49023
O=CO			1	0	2	39863
c1ccncc1			3	2	4	15115
c1nc2nc[nH]c2n1			7	3	6	11369
NS(=O)=O			1	0	2	10121
O=P(O)(O)O			1	0	2	7451
OCO			1	0	2	6405
c1cncnc1			3	2	4	5965
c1cn[nH]c1			2	3	1	5404

Smiles	2D graph	3D structures	A	B	C	T
<chem>O=P(O)O</chem>			0	1	center(2,3)	5271
<chem>c1ccc2ccccc2c1</chem>			3	2	4	4742
<chem>c1ccsc1</chem>			3	2	4	4334
<chem>N=CN</chem>			1	0	2	4315
<chem>NC(N)=O</chem>			2	1	3	4167
<chem>O=c1cc[nH]c(=O)[nH]1</chem>			7	1	5	4145
<chem>c1ccc2ncccc2c1</chem>			3	2	4	3519
<chem>c1cscn1</chem>			2	3	1	3466
<chem>c1ccc2[nH]cnc2c1</chem>			5	4	6	3462
<chem>c1c[nH]cn1</chem>			3	2	4	2964
<chem>O=[N+][O-]</chem>			1	0	2	2702
<chem>O=CNO</chem>			1	0	2	2477
<chem>NC(=O)O</chem>			1	0	2	2438
<chem>O=S=O</chem>			1	0	2	2375
<chem>c1ccc2[nH]ccc2c1</chem>			3	4	2	2301

B.2 LBE ANALYSIS

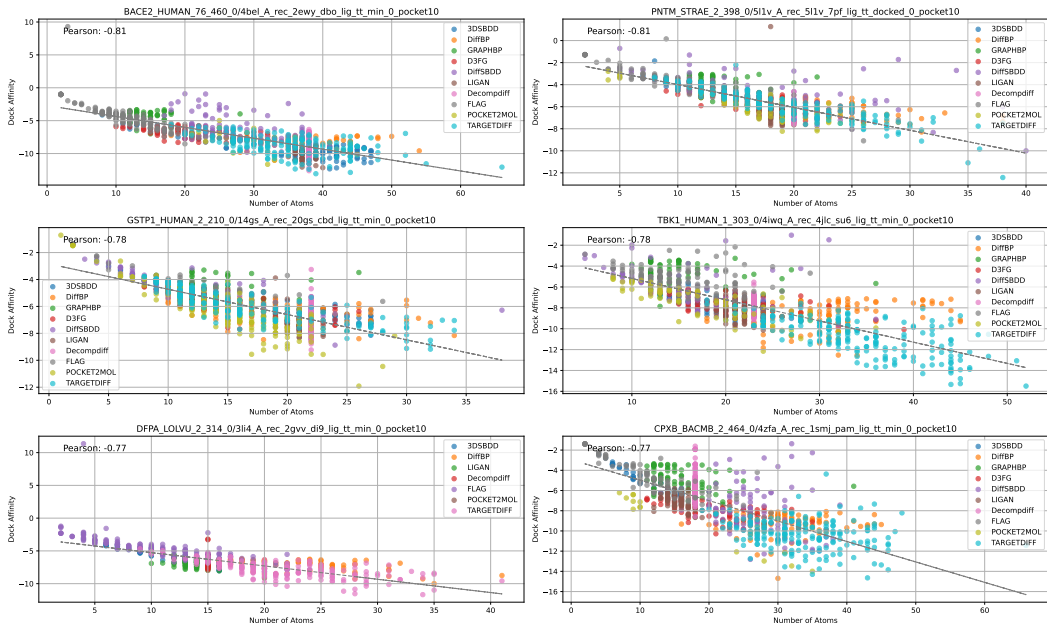


Figure 6: A demonstration of how the molecule size affects the binding energy. The 6 pockets that are most linear-correlated with atom number.

B.3 METRIC CALCULATION

The metric of MPBG can be written as $MPBG_j = \text{Mean}_i(\frac{E_{i, \text{gen}} - E_{\text{ref}}}{E_{\text{ref}}} \times 100\%)$, in which i is the indicator of the generated molecules in a single protein and $\text{Mean}_i(\cdot)$ calculates average along indicator i , with $MPBG = \text{Mean}_j(MPBG_j)$. The MPBG is a per-pocket metric that is calculated within a single pocket, which differs from other averaging metrics.

For chemical property calculation, we use functions in `RDKit` (`RDKit`, online), and note that the SA is the normalized one employed in the previous studies.

For interaction pattern analysis, we employ `PLIP`, which considers 7 kinds of interaction types including ‘hydrophobic interactions’, ‘hydrogen bonds’, ‘water bridges’, ‘ π -stacks’, ‘ π -cation interactions’, ‘halogen bonds’ and ‘metal complexes’.

For MAE metrics that are related to the molecule sizes, the generative model tends to achieve higher scores when the atom number is close to that of the reference. We suppose it is reasonable, considering that the size of the molecule itself is determined by factors such as the size and shape of the pocket, and these characteristics should be captured by the models.

B.4 DISCUSSION ON LBE.

- Is it possible that smaller molecules exhibit higher efficacy, thus leading LBE to be meaningless? (Reynolds et al., 2008)

Meaning. The introduction of Ligand Binding Efficiency (LBE) is motivated by observations in Appendix B.2, where we identified a strong positive correlation between the size of the generated molecules and the Vina docking energy. To address this size-related bias, LBE was incorporated as an additional metric. This approach is consistent with the basic principles of energy calculation, where the total binding energy is derived from the sum of interaction energies contributed by each atom, i.e. $E_{\text{vina}} \sim E_{\text{bind}} = \sum_{i=1}^{N_{\text{atom}}} E_i$. Thus, using LBE as a measure of the average per-atom contribution to binding affinity is both logical and appropriate, as $LBE = -\frac{E_{\text{bind}}}{N_{\text{atom}}}$. Furthermore,

Table 11: Ratio of generated molecule’s size and the corresponding LBE.

Method	Mol Size	[1,3]	(3,10]	(10,20]	(20,30]	>30
LiGAN	Ratio(%)	0.01	13.61	40.09	36.77	9.59
	LBE	0.37	0.42	0.44	0.35	0.30
3DSBDD	Ratio(%)	0.01	15.48	54.44	22.63	7.42
	LBE	0.39	0.42	0.41	0.33	0.31
GRAPHBP	Ratio(%)	0.00	0.77	91.29	6.07	1.84
	LBE	-	0.36	0.33	0.21	0.20
POCKET2MOL	Ratio(%)	0.08	24.22	48.83	20.19	6.64
	LBE	0.43	0.45	0.44	0.33	0.30
TARGETDIFF	Ratio(%)	0.00	10.24	28.17	39.51	22.05
	LBE	-	0.44	0.44	0.31	0.29
DIFFSBDD	Ratio(%)	0.13	21.54	41.43	28.01	8.86
	LBE	0.37	0.38	0.30	0.24	0.22
DIFFBP	Ratio(%)	0.00	7.29	32.19	43.08	17.42
	LBE	-	0.41	0.42	0.31	0.29
FLAG	Ratio(%)	0.04	39.01	54.29	6.52	0.13
	LBE	0.40	0.35	0.33	0.24	0.19
D3FG	Ratio(%)	0.00	8.31	61.70	27.72	2.55
	LBE	-	0.44	0.45	0.32	0.25
DECOMPDIF	Ratio(%)	0.00	9.99	35.50	33.98	20.51
	LBE	-	0.38	0.38	0.33	0.30
MOLCRAFT	Ratio(%)	0.00	9.18	30.97	39.62	20.21
	LBE	-	0.44	0.41	0.33	0.29
VOXBIND	Ratio(%)	0.00	6.10	36.64	43.39	15.85
	LBE	-	0.43	0.41	0.34	0.26

numerous studies in medicinal chemistry have highlighted Ligand Efficiency as a critical evaluation criterion, advocating for its widespread use as an effective metric for assessing molecular binding affinity (Hopkins et al., 2014b; Kenny, 2017; Murray et al., 2010).

Reasonability. It can be usually concluded from Reynolds et al. (2008) that ‘smaller molecules tend to have higher LBE’, while we believe this conclusion is incorrect. We claim that different protein pockets exhibit a preference for molecule sizes. If this conclusion were true, it would imply that molecules consisting of a single atom would have the optimal LBE? To explore this issue, in Table. 11, we give statistics of molecule sizes v.s. LBE of methods evaluated. It shows that such molecules with extreme sizes (less than 4) that make the LBE meaningless are scarcely generated since they have a small ratio. Ligands with sizes less than 20 usually have better LBE because of the preference of the pockets, as a consequence of protein binding sites being limited in their size, thus generating the preference of binding molecules’ sizes. Larger ligand with sizes of more than 20 gets decreased LBE because it becomes increasingly difficult to form optimal interactions with every site on the protein without introducing unfavorable ligand strain.

Little Effects of Extreme Samples. Besides, we use a weighted ranking with equal weights as previous benchmarks (Wang et al., 2022), to give an unbiased evaluation. Given that LBE accounts for one-twelfth of the total weight in interaction analysis, the impact of failed samples in LBE on calculating the LBE metrics and final ranking is minimal. Therefore, we claim that the inclusion of a minimal number of invalid LBE calculations will not render the overall ranking ineffective.

B.5 PREVIOUSLY-USED METRICS FOR EVALUATION

The aspects of evaluation are commonly used with different methods, while they hardly give a very comprehensive evaluation. We give a brief review of each method’s evaluation on these aspects in Table. 12.

C CODEBASE STRUCTURE

In this section, we provide an overview of the codebase structure of CBGBench, where four abstract layers are adopted. The layers include the core layer, algorithm layer, chemistry layer, and API layer in the bottom-up direction as shown in Fig. 7. This codebase is licensed under the Apache License,

Table 12: Different methods’ evaluation aspects in the published papers.

Method	Substructure	Geometry	Chem Property	Interaction
LiGAN	Figure. S6	Figure. S7, S8, S9	Figure. 3, S3, S4, S5	Figure. S13, S14
POCKET2MOL	Table. 2	Table. 3; Figure. 4	Table. 1	Table. 1
GRAPHBP	-	Table. 2; Figure. 5	-	Table. 1; Figure. 2
TARGETDIFF	Table. 2	Table. 1; Figure. 2	Table. 3	Table. 3, Figure. 4
DIFFBP	Table. 3	-	Table. 2	Table. 1
DIFFSBDD	-	Figure. 8, 9	Table. 1	Table. 1, 2; Figure. 2
FLAG	Table. 3	Table. 2; Figure. 4	Table. 1	Table. 1
D3FG	Table. 1, 3; Figure. 3	Table. 2	Table. 4	Table. 4
DECOMPDIFF	-	Table. 1, 2; Figure. 3	Table. 3	Table. 3
MOLCRAFT	Table. 1	Table. 2	Table. 2	Table. 2
VOXBIND	-	Figure. 7	Table. 1	Table. 1; Figure. 5

Version 2.0. It provides a robust and flexible framework for building and evaluating graph neural network models for structure-based drug design and lead optimization.

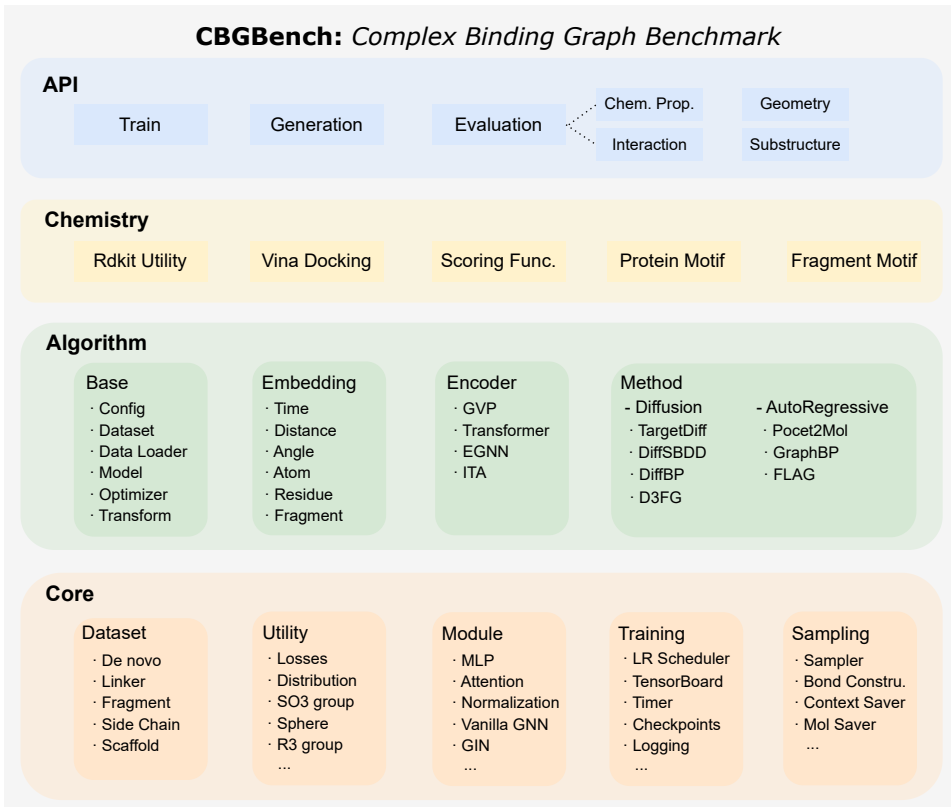


Figure 7: Structure of CBGBench Codebase, consisting of 4 layers. The core layer provides the common functions, datasets, and modules for CBG methods. The algorithm layer mainly implements the prevailing CBG algorithms. The Chemistry layer is used for data preprocessing and evaluation.

Core Layer. In the core layer, we implement the commonly used core functions for training and sampling CBG algorithms. Besides, the code regarding datasets, data loaders, and basic modules used in CBGBench is also provided in the core layer.

Algorithm Layer. In the algorithm layer, we first implement the base class for CBG algorithms, where we initialize the datasets, data loaders, and basic modules from the core layer. We modularize each method, first using embedding layers to project the input into high-dimensional space, and then employing different 3D equivariant GNNs to construct the algorithm, including Diffusion-based and Auto-regressive-based ones. We further abstract the algorithms, enabling better code reuse and making it easier to implement new algorithms. The voxel-based methods are not included because

our framework is mostly based on EGNs, which will be added to the codebase as future work, and DecompDiff requires different data preprocessing. Based on this, we support 7 core CBG algorithms. More algorithms are expected to be added through continued extension.

Chemistry Layer. The chemistry layer is mostly built with post-processing utilities and evaluators such as atom type, bond angle, and docking modules. Besides, several prior decomposition functions are used as molecule parsers, and the molecule and protein fragment motifs serve as prior knowledge.

API Layer. We wrap the core functions and algorithms in CBGBench in the API layer as a public Python package. It is friendly for users from different backgrounds who want to employ CBG algorithms in new applications. Training and sampling can be done in only a few lines of code. In addition, we provide the configuration files of all algorithms supported in CBGBench with detailed parameter settings, allowing the reproduction of the results.

D EXPERIMENTAL IMPLEMENTATION DETAILS

Experiments are conducted based on Pytorch 2.0.1 on a hardware platform with Intel(R) Xeon(R) Gold 6240R @ 2.40GHz CPU and NVIDIA A100 GPU. We give the detailed parameters for training the included models in Table. 13. Note that most of the hyperparameters’ combinations are directly the officially-provided ones. Specifically, The methods included in our codebase are either self-trained or trained by us when the official repository does not provide a pretrained checkpoint. For methods that are not included, we validate them using the pretrained models that have been provided. In the Lead-Optimization tasks, the finetuning parameters are the same.

Table 13: The hyper-parameters in for training and sampling molecules for the SBDD methods. Different from GNN-based methods, CNN-based methods usually have a different hidden dimension size, so we report the highest ones. ‘Num steps’ are the sampling steps which is usually used in diffusion-based methods, including DDPMs and BFNs. For other hyper-parameters in detail, please read the config files provided in the supplementary materials from `./configs/denovo/train`.

Method	Batch Size	Hidden Dim	Layer num	Learning rate	Optimizer	Num Steps
LIGAN	8	128	4	1E-05	RMSprop	/
3DSBDD	4	256	6	1E-04	Adam	/
GRAPHBP	16	64	6	1E-04	Adam	/
POCKET2MOL	8	256	6	1E-05	Adam	/
TARGETDIFF	4	128	9	5E-04	Adam	1000
DIFFSBDD	16	256	6	1E-03	Adam	500
DIFFBP	16	256	6	1E-04	Adam	1000
FLAG	4	256	6	1E-04	Adam	/
D3FG	16	128	6	1E-04	Adam	1000
DECOMPDIFF	4	128	6	5E-04	Adam	1000
MOLCRAFT	8	128	9	5E-04	Adam	1000
VOXBIND	32	512	4	1E-05	AdamW	100

E EXPERIMENTAL RESULT DETAILS

E.1 DE NOVO GENERATION

E.1.1 SUBSTRUCTURE

Table. 14 gives the generated molecules’ atom distribution in detail. It shows DIFFBP and GRAPHBP tend to generate more C atoms and have a low probability of generating uncommon atoms. In contrast, D3FG and FLAG, which directly use a motif library, have a higher probability of generating these uncommon atoms. Table. 15 gives the generated molecules’ ring distribution in detail. DIFFBP and DIFFSBDD perform poorly due to significant inconsistencies in generating large complex fragments. For example, they also generate a large number of unreasonable triangular and tetrahedral rings. Similarly, these methods also fall short in generating complex functional groups, as shown in Table. 16. This leads to their subpar performance in substructure generation.

Table 14: Distribution of different atom types across different methods.

Method	C	N	O	F	P	S	Cl
REF.	0.6715	0.1170	0.1696	0.0131	0.0111	0.0112	0.0064
LiGAN	0.6477	0.0775	0.2492	0.0005	0.0224	0.0019	0.0008
3DSBDD	0.6941	0.1311	0.1651	0.0025	0.0063	0.0010	0.0000
GRAPHBP	0.8610	0.0397	0.0868	0.0036	0.0040	0.0039	0.0010
POCKET2MOL	0.7623	0.0855	0.1413	0.0025	0.0044	0.0027	0.0013
TARGETDIFF	0.6935	0.0896	0.1924	0.0110	0.0059	0.0052	0.0025
DIFFSBDD	0.7000	0.1154	0.1611	0.0081	0.0017	0.0093	0.0031
DIFFBP	0.9178	0.0030	0.0792	0.0000	0.0000	0.0000	0.0000
FLAG	0.5585	0.1341	0.2077	0.0265	0.0312	0.0347	0.0074
D3FG	0.7336	0.1158	0.1286	0.0056	0.0035	0.0088	0.0040
DECOMPDIFF	0.6762	0.0978	0.1927	0.0064	0.0149	0.0088	0.0033
MOLCRAFT	0.6735	0.0917	0.2056	0.0103	0.0094	0.0058	0.0035
VOXBIND	0.7359	0.1083	0.1390	0.0000	0.0046	0.0120	0.7382

Table 15: Distribution of different ring sizes across various methods.

Method	3	4	5	6	7	8
REF.	0.0130	0.0020	0.2855	0.6894	0.0098	0.0003
LiGAN	0.2238	0.0698	0.2599	0.4049	0.0171	0.0096
3DSBDD	0.2970	0.0007	0.1538	0.5114	0.0181	0.0116
GRAPHBP	0.0000	0.2429	0.1922	0.1765	0.1533	0.1113
POCKET2MOL	0.0000	0.1585	0.1822	0.4373	0.1410	0.0478
TARGETDIFF	0.0000	0.0188	0.2856	0.4918	0.1209	0.0298
DIFFSBDD	0.2842	0.0330	0.2818	0.2854	0.0718	0.0193
DIFFBP	0.0000	0.2195	0.2371	0.2215	0.1417	0.0707
FLAG	0.0000	0.0682	0.2716	0.5228	0.0996	0.0231
D3FG	0.0000	0.0201	0.2477	0.5966	0.0756	0.0283
DECOMPDIFF	0.0302	0.0378	0.3407	0.4386	0.1137	0.0196
MOLCRAFT	0.0000	0.0022	0.2494	0.6822	0.0489	0.0072
VOXBIND	0.0000	0.0062	0.2042	0.7566	0.0232	0.0021

Table 16: Distribution of the top ten functional groups across different methods.

Method	c1ccccc1	NC=O	O=CO	c1ccncc1	c1ncc2nc[nH]c2n1	NS(=O)=O	O=P(O)(O)O	OCO	c1cncnc1	c1cn[nH]c1
REF.	0.3920	0.1465	0.1192	0.0452	0.0340	0.0303	0.0223	0.0191	0.0178	0.0162
LiGAN	0.3464	0.0998	0.1549	0.0546	0.1028	0.0127	0.0490	0.0897	0.0197	0.0000
3DSBDD	0.3109	0.1488	0.1219	0.0769	0.0090	0.0000	0.0814	0.0915	0.0148	0.0291
GRAPHBP	0.0133	0.1330	0.1888	0.0000	0.0000	0.0000	0.0000	0.6064	0.0000	0.0000
POCKET2MOL	0.3794	0.1098	0.2906	0.0305	0.0000	0.0000	0.0150	0.0964	0.0030	0.0000
TARGETDIFF	0.2729	0.1520	0.3085	0.0427	0.0001	0.0000	0.0241	0.0855	0.0069	0.0065
DIFFSBDD	0.0073	0.1985	0.5787	0.0194	0.0000	0.0073	0.0000	0.0145	0.0000	0.0000
DIFFBP	0.1962	0.0108	0.4440	0.0010	0.0000	0.0000	0.0000	0.3289	0.0000	0.0000
FLAG	0.2223	0.1880	0.1736	0.0365	0.0009	0.0000	0.0014	0.2471	0.0135	0.0014
D3FG	0.3002	0.1597	0.2078	0.0323	0.0114	0.0000	0.0212	0.0751	0.0410	0.0000
DECOMPDIFF	0.3173	0.1660	0.2125	0.0527	0.0094	0.0057	0.0418	0.0443	0.0134	0.0128
MOLCRAFT	0.3960	0.1798	0.2361	0.0377	0.0001	0.0000	0.0362	0.0344	0.0053	0.0002
VOXBIND	0.4705	0.1138	0.1663	0.0762	0.0001	0.0000	0.0191	0.0334	0.0110	0.0000

E.1.2 INTERACTION

PLIP Interaction Pattern. Table. 17 and 18 provide detailed interaction pattern analysis. Most models captured good interaction patterns, generating a substantial amount of hydrophobic and hydrogen interactions. DiffSBDD excessively generated hydrophobic interactions. Additionally, for interactions such as π -stacking, π -cation, and halogen interactions, which do not exist in the reference molecules, the models could probabilistically generate molecules capable of producing such interactions with the protein.

E.1.3 GEOMETRY

Here we give detailed bond length and bond angle distribution of the evaluated method’s generated molecules and the reference, in Table. 19 and 20. It shows that the

E.2 LEAD OPTIMIZATION

We here give the details of interaction analysis. Since these tasks have provided a partial of the molecules as the context, it is hard to tell the superiority of generated substructures or geometries. Table. 21 and 22 gives details. it shows that

- The optimization on the side chains has the least effect on the interaction pattern in an overall result and has the greatest influence on the linker.

Table 17: Frequency of interaction type.

Method	hydrophobic	hydrogen	water bridge	π -stacks	π -cation	halogen	metal
REF.	3.0000	3.0000	0.0000	0.0000	0.0000	0.0000	0.0000
LiGAN	3.1354	3.5078	0.0000	0.1045	0.0441	0.0034	0.0000
3DSBDD	3.1237	3.0853	0.0000	0.1405	0.0434	0.0053	0.0000
GRAPHBP	5.2008	0.8039	0.0000	0.0007	0.0046	0.0060	0.0000
POCKET2MOL	4.9366	1.8840	0.0000	0.0176	0.0081	0.0045	0.0000
TARGETDIFF	4.2444	3.5309	0.0000	0.1159	0.0377	0.0384	0.0000
DIFFSBDD	3.9009	3.3202	0.0000	0.0986	0.0338	0.0279	0.0000
DIFFBP	4.1027	1.4830	0.0000	0.0213	0.0039	0.0000	0.0000
FLAG	1.9319	2.1490	0.0000	0.0134	0.0185	0.0528	0.0000
D3FG	4.3149	2.4718	0.0000	0.0607	0.0260	0.0200	0.0000
DECOMPDIFF	3.9284	3.4531	0.0000	0.1177	0.0436	0.0290	0.0000
MOLCRAFT	4.0147	3.9456	0.0000	0.2038	0.0667	0.0377	0.0000
VOXBIND	4.4920	2.8395	0.0000	0.1659	0.0599	0.0001	0.0000

Table 18: Distribution of interaction type.

Method	hydrophobic	hydrogen	water bridge	π -stacks	π -cation	halogen	metal
REF.	0.5000	0.5000	0.0000	0.0000	0.0000	0.0000	0.0000
LiGAN	0.4614	0.5162	0.0000	0.0154	0.0065	0.0005	0.0000
3DSBDD	0.4882	0.4822	0.0000	0.0220	0.0068	0.0008	0.0000
GRAPHBP	0.8645	0.1336	0.0000	0.0001	0.0008	0.0010	0.0000
POCKET2MOL	0.7206	0.2750	0.0000	0.0026	0.0012	0.0007	0.0000
TARGETDIFF	0.5327	0.4432	0.0000	0.0146	0.0047	0.0048	0.0000
DIFFSBDD	0.5285	0.4498	0.0000	0.0134	0.0046	0.0038	0.0000
DIFFBP	0.6579	0.3398	0.0000	0.0020	0.0004	0.0000	0.0000
FLAG	0.4638	0.5159	0.0000	0.0032	0.0045	0.0127	0.0000
D3FG	0.6259	0.3586	0.0000	0.0088	0.0038	0.0029	0.0000
DECOMPDIFF	0.5188	0.4560	0.0000	0.0155	0.0058	0.0038	0.0000
MOLCRAFT	0.4855	0.4771	0.0000	0.0246	0.0080	0.0045	0.0000
VOXBIND	0.5943	0.3757	0.0000	0.0219	0.0007	0.0212	0.0000

Table 19: JSD Bond Length Comparisons across different methods.

METHOD	C-C	C-N	C-O	C=C	C=N	C=O
LiGAN	0.4986	0.4146	0.4560	0.4807	0.4776	0.4595
3DSBDD	0.2090	0.4258	0.5478	0.5170	0.6701	0.6448
GRAPHBP	0.5038	0.4231	0.4973	0.6235	0.4629	0.5986
POCKET2MOL	0.5667	0.5698	0.5433	0.4787	0.5989	0.5025
TARGETDIFF	0.3101	0.2490	0.3072	0.1715	0.1944	0.3629
DIFFSBDD	0.3841	0.3708	0.3291	0.3043	0.3473	0.3647
DIFFBP	0.5704	0.5256	0.5090	0.6161	0.6314	0.5296
FLAG	0.3460	0.3770	0.4433	0.4872	0.4464	0.4292
D3GF	0.4244	0.3227	0.3895	0.3860	0.3570	0.3566
DECOMPDIFF	0.2562	0.2007	0.2361	0.2590	0.2844	0.3091
MOLCRAFT	0.2473	0.1732	0.2341	0.3040	0.1459	0.2250
VOXBIND	0.3335	0.2577	0.3507	0.1991	0.1459	0.3334

Table 20: JSD Bond Angle Comparisons across different methods.

JSD _{BA}	LiGAN	3DSBDD	GRAPHBP	POCKET2MOL	TARGETDIFF	DIFFSBDD	DIFFBP	FLAG	D3GF	DECOMPDIFF	MOLCRAFT	VOXBIND
C#C-C	0.6704	0.4838	0.7507	0.6477	0.6845	0.6788	0.7204	0.4591	0.7027	0.8174	0.4922	0.6275
C-C#N	0.8151	0.2980	0.8326	0.5830	0.7437	0.7388	0.7928	0.3461	0.7120	0.7254	0.2252	0.7320
C-C-C	0.5260	0.2189	0.5015	0.4663	0.2955	0.3825	0.5234	0.3439	0.3703	0.2306	0.1926	0.2742
C-C-N	0.5102	0.2934	0.4975	0.4790	0.2738	0.4265	0.5189	0.3650	0.3592	0.1987	0.1097	0.2280
C-C-O	0.5198	0.3279	0.5216	0.5078	0.3335	0.3930	0.5327	0.3710	0.4021	0.2124	0.1277	0.3233
C-C=C	0.4657	0.2701	0.4430	0.2826	0.1815	0.3163	0.5047	0.2830	0.2706	0.2215	0.2267	0.1823
C-C=N	0.4441	0.4159	0.4376	0.3507	0.2075	0.3185	0.5171	0.3353	0.3205	0.2094	0.3175	0.2707
C-N-C	0.5209	0.3176	0.4586	0.3981	0.2915	0.4168	0.5378	0.4237	0.3597	0.1952	0.1475	0.1532
C-N-N	0.5889	0.2847	0.5403	0.4997	0.2626	0.4022	0.6005	0.4161	0.3505	0.2825	0.2702	0.1813
C-N-O	0.7019	0.4996	0.6338	0.6173	0.3263	0.4653	0.7070	0.5560	0.4943	0.3120	0.2002	0.3300
C-N=C	0.3646	0.4011	0.5133	0.3728	0.3105	0.3191	0.4433	0.4085	0.4517	0.3467	0.4092	0.3626
C-N=N	0.3597	0.6214	0.7639	0.7062	0.4400	0.4212	0.8326	0.7023	0.7380	0.3917	0.6954	0.7196
C-O-C	0.5111	0.4259	0.4872	0.4204	0.2865	0.3786	0.5478	0.4606	0.3765	0.1882	0.1113	0.3305
C-O-N	0.7893	0.3465	0.6637	0.6140	0.4312	0.5485	0.7520	0.6257	0.4988	0.4064	0.3336	0.4436
C=C-N	0.4580	0.4140	0.5415	0.3732	0.2359	0.3223	0.4075	0.3361	0.3226	0.2574	0.1760	0.2905
C=C=C	0.7593	0.6866	0.7793	0.7373	0.7445	0.7549	0.7752	0.7419	0.7603	0.7703	0.6388	0.8326
N#C-C	0.8151	0.2980	0.8326	0.5830	0.7437	0.7388	0.7928	0.3461	0.7120	0.7254	0.2252	0.7320
N-C-N	0.5157	0.3795	0.4179	0.5544	0.3058	0.4409	0.6764	0.4316	0.4464	0.2994	0.2604	0.2569
N-C-O	0.4713	0.2673	0.6054	0.5879	0.3926	0.4346	0.5923	0.4089	0.4987	0.3029	0.2612	0.4190
N-C=N	0.4598	0.3670	0.3450	0.3986	0.2175	0.3558	0.5498	0.2654	0.3531	0.2593	0.1366	0.1360
N-C=O	0.5275	0.3900	0.4285	0.2347	0.2664	0.3690	0.5719	0.3636	0.3695	0.1197	0.0378	0.2508
N-N-O	0.8326	0.6048	0.7791	0.7639	0.5862	0.5912	0.7447	0.7117	0.6875	0.4831	0.6708	0.5859
N=C-N	0.4598	0.3670	0.3450	0.3986	0.2175	0.3558	0.5498	0.2654	0.3531	0.2593	0.1366	0.1360
O=C-N	0.5275	0.3900	0.4285	0.2347	0.2664	0.3690	0.5719	0.3636	0.3695	0.1197	0.0378	0.2508

- GRAPHBP’s failure in scaffold hopping also can be reflected by the fact that the interaction pattern cannot be produced with the molecules.

Table 21: Frequency of interaction type on lead optimization tasks.

	Method	hydrophobic	hydrogen	water bridge	π -stacks	π -cation	halogen	metal
	REF.	3.0000	3.0000	0.0000	0.0000	0.0000	0.0000	0.0000
Linker	GRAPHBP	5.5795	2.9812	0.0000	0.5362	0.3537	0.0000	0.0000
	POCKET2MOL	5.1879	3.2759	0.0000	0.1708	0.1082	0.0326	0.0000
	TARGETDIFF	5.3811	3.7133	0.0000	0.1675	0.0827	0.0404	0.0000
	DIFFSBDD	5.4132	3.1350	0.0000	0.1153	0.0132	0.0308	0.0000
	DIFFBP	7.0697	2.6017	0.0000	0.1226	0.0678	0.0204	0.0000
Fragment	GRAPHBP	3.0084	3.2071	0.0000	0.0947	0.0499	0.0196	0.0000
	POCKET2MOL	4.4064	4.0854	0.0000	0.1238	0.0956	0.0131	0.0000
	TARGETDIFF	4.3187	3.6436	0.0000	0.1040	0.0648	0.0405	0.0000
	DIFFSBDD	4.3086	3.6720	0.0000	0.1087	0.0089	0.0468	0.0000
	DIFFBP	5.6128	2.7838	0.0000	0.0552	0.0339	0.0175	0.0000
Side Chain	GRAPHBP	3.0173	1.2207	0.0000	0.2029	0.0321	0.0001	0.0000
	POCKET2MOL	3.0643	3.8911	0.0000	0.0872	0.0708	0.0194	0.0000
	TARGETDIFF	3.3468	3.6206	0.0000	0.0975	0.0527	0.0851	0.0000
	DIFFSBDD	3.6822	3.3479	0.0000	0.0271	0.0242	0.0098	0.0000
	DIFFBP	4.5444	2.5941	0.0000	0.0696	0.0349	0.0141	0.0000
Scaffold	GRAPHBP	0.9560	2.3953	0.0000	0.0000	0.0007	0.0007	0.0000
	POCKET2MOL	3.2220	3.4761	0.0000	0.0282	0.0295	0.0246	0.0000
	TARGETDIFF	3.5427	4.1047	0.0000	0.0612	0.0383	0.0303	0.0000
	DIFFSBDD	4.6225	3.2649	0.0000	0.0021	0.0138	0.1786	0.0000
	DIFFBP	5.0840	2.4424	0.0000	0.0061	0.0055	0.0110	0.0000

Table 22: Distribution of interaction type on lead optimization tasks.

	Method	hydrophobic	hydrogen	water bridge	π -stacks	π -cation	halogen	metal
	REF.	0.5000	0.5000	0.0000	0.0000	0.0000	0.0000	0.0000
Linker	GRAPHBP	0.5904	0.3154	0.0000	0.0567	0.0374	0.0000	0.0000
	POCKET2MOL	0.5912	0.3733	0.0000	0.0195	0.0123	0.0037	0.0000
	TARGETDIFF	0.5734	0.3957	0.0000	0.0178	0.0088	0.0043	0.0000
	DIFFSBDD	0.6216	0.3600	0.0000	0.0132	0.0015	0.0035	0.0000
	DIFFBP	4.1027	1.4830	0.0000	0.0213	0.0039	0.0021	0.0000
Fragment	GRAPHBP	0.4716	0.5027	0.0000	0.0148	0.0078	0.0031	0.0000
	POCKET2MOL	0.5051	0.4683	0.0000	0.0142	0.0110	0.0015	0.0000
	TARGETDIFF	0.5285	0.4459	0.0000	0.0127	0.0079	0.0050	0.0000
	DIFFSBDD	0.5289	0.4508	0.0000	0.0133	0.0011	0.0057	0.0000
	DIFFBP	0.6601	0.3274	0.0000	0.0065	0.0040	0.0021	0.0000
Side Chain	GRAPHBP	0.6746	0.2729	0.0000	0.0454	0.0072	0.0000	0.0000
	POCKET2MOL	0.4296	0.5455	0.0000	0.0122	0.0099	0.0027	0.0000
	TARGETDIFF	0.4647	0.5027	0.0000	0.0135	0.0073	0.0118	0.0000
	DIFFSBDD	0.5192	0.4721	0.0000	0.0038	0.0034	0.0013	0.0000
	DIFFBP	0.6262	0.3575	0.0000	0.0096	0.0048	0.0019	0.0000
Scaffold	GRAPHBP	0.2851	0.7144	0.0000	0.0000	0.0002	0.0002	0.0000
	POCKET2MOL	0.4752	0.5127	0.0000	0.0042	0.0043	0.0036	0.0000
	TARGETDIFF	0.4555	0.5278	0.0000	0.0079	0.0049	0.0039	0.0000
	DIFFSBDD	0.5719	0.4039	0.0000	0.0003	0.0017	0.0221	0.0000
	DIFFBP	0.6735	0.3235	0.0000	0.0008	0.0007	0.0015	0.0000

E.3 CASE STUDY

DRD3. For DRD3, we give the distribution of different models’ generated molecules in chemical space in Figure. 8. Different methods capture different clustering centers of the actives, while their distributions show a great gap from the GEOM-DRUG’s randomly sampled molecules.

E.4 VALIDITY

Validity is an important metric to evaluate whether the molecules generated by the models are valid. There are two methods to reconstruct the 3D positions of the atoms into a molecule with bonds, one is used in TARGETDIFF, POCKET2MOL and 3DSBDD, which we name as *Refine*; The second is to use *Openbabel* (Open Babel development team) the software, used in DIFFSBDD. However, using these methods to reconstruct molecules always carries the risk of broken bonds, which makes the strategy of selecting connected atoms to form fragments and ultimately the final molecule crucial. Here, we define a chemically valid molecule as one where the number of atoms in the largest fragment is greater than 85% of the total number of atoms, and we use this as the criterion for the reconstruction. Additionally, we employed a ‘*Refine + Openbabel*’ strategy, where if refinement is unsuccessful, Openbabel is added as a reconstruction method. Under this definition, the validity of various methods in the *de novo* task is shown in Table. 23. *DecompDiff* and *TargetDiff* have the highest validity.

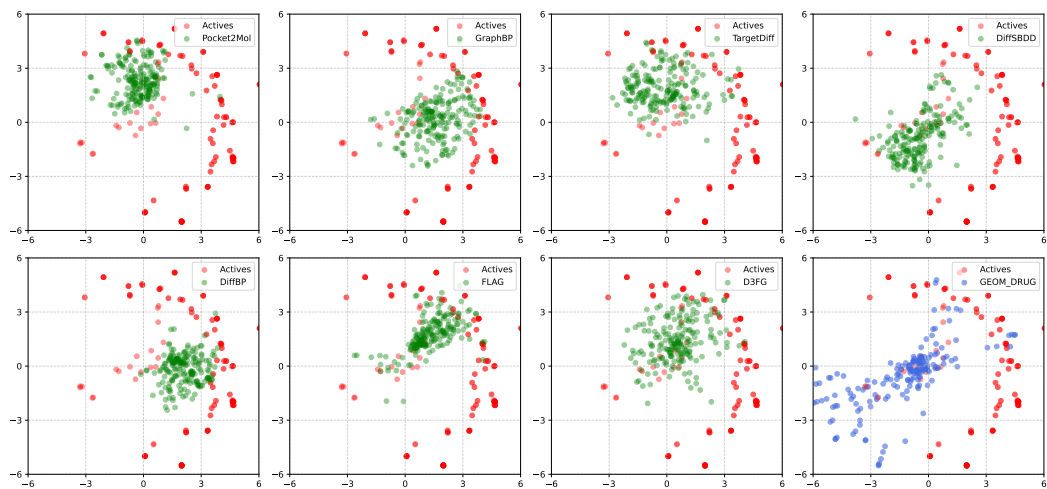


Figure 8: T-SNE visualization of chemical distributions of generated and active molecules on t-SNE.

Table 23: Denovo Validity and Rank

Method	Validity	Rank
LiGAN	0.42	12
3DSBDD	0.54	11
GraphBP	0.66	10
Pocket2Mol	0.75	6
TargetDiff	0.96	1
DiffSBDD	0.71	7
DiffBP	0.78	4
FLAG	0.68	9
D3FG	0.77	5
DecompDiff	0.89	3
MolCraft	0.95	2
VoxBind	0.74	8